NATIONAL ENERGY TECHNOLOGY LABORATORY

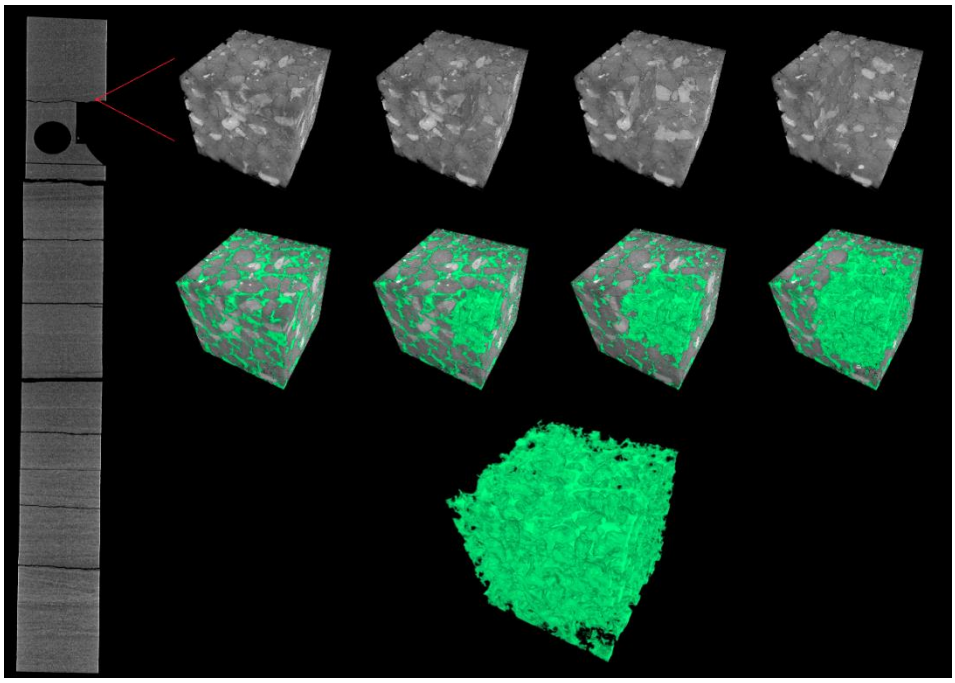

Computed Tomography Scanning and Geophysical Measurements of the One Earth Energy Well #1 Core

27 March 2023

U.S. DEPARTMENT OF ENERGY | NATIONAL ENERGY TECHNOLOGY LABORATORY

Office of Fossil Energy and Carbon Management

DOE/NETL-2023/3847

Disclaimer

Cover Illustration: Computed tomography images from the One Earth Energy Well #1 from a depth of 6,344 ft. Left: Medical CT image of core from 6,344 to 6,347 ft. Right Top: Micro-CT images of a $(2\ mm)^3$ cube of rock from ~6,344 ft. Micro CT images have been processed to isolate the open pore space (green) and volumes of the cube have been removed to illustrate the connectivity. Right Bottom: Isolated pore space in the micro-CT $(2\ mm)^3$ cube.

Suggested Citation: Crandall, D.; Gill, M.; Paronish, T.; Brown, S.; Mitchell, N.; Jarvis, K.; Moore, J.; Blakley, C.; Okwen, R.; Korose, C.; Carman, C. *Computed Tomography Scanning and Geophysical Measurements of the One Earth Energy Well #1 Core;* DOE.NETL-2023.3847; NETL Technical Report Series; U.S. Department of Energy, National Energy Technology Laboratory: Morgantown, WV, 2023; p 60. https://doi.org/10.2172/1963265

An electronic version of this report can be found at:

https://netl.doe.gov/energy-analysis/search

https://edx.netl.doe.gov/carbonstorage

The data in this report can be accessed from NETL's Energy Data eXchange (EDX) online system (https://edx.netl.doe.gov) using the following link: https://edx.netl.doe.gov/dataset/illinois-storage-corridor-one-earth-energy-1-core

Computed Tomography Scanning and Geophysical Measurements of the One Earth Energy Well #1 Core

Dustin Crandall[1], Magdalena Gill[1,2], Thomas Paronish[1,2], Sarah Brown[1,2], Natalie Mitchell[1,2], Karl Jarvis[1,2], Johnathan Moore[1], Curt Blakley[3], Roland Okwen[3], Christopher Korose[3], Carl Carman[3]

[1]U.S. Department of Energy, National Energy Technology Laboratory, 3610 Collins Ferry Road, Morgantown, WV 26505

[2]NETL Support Contractor, 3610 Collins Ferry Road, Morgantown, WV 26505

[3]Illinois State Geological Survey, 615 E. Peabody, Champaign, IL 61820

DOE/NETL-2023/3847

27 March 2023

NETL Contacts:

Dustin Crandall, Principal Investigator and Technical Portfolio Lead

Bryan Morreale, Associate Laboratory Director for Research & Innovation, Research & Innovation Center

This page intentionally left blank.

Table of Contents

This page intentionally left blank.

List of Figures

List of Figures (cont.)

List of Tables

This page intentionally left blank.

Acronyms, Abbreviations, and Symbols

Term	Description
2D	Two-dimensional
CO_2	Carbon Dioxide
CT	Computed tomography
DOE	Department of Energy
EDX	NETL's Energy Data eXchange
ISC	Illinois Storage Corridor
ISGS	Illinois State Geological Survey
MSCL	Multi-Sensor Core Logger
NETL	National Energy Technology Laboratory
OEE	One Earth Energy
XRF	X-ray fluorescence

Acknowledgments

This work was completed at the National Energy Technology Laboratory (NETL) with support from the U.S. Department of Energy's (DOE) Office of Fossil Energy and Carbon Management. The authors wish to acknowledge Bryan Morreale (NETL Research & Innovation Center), William Aljoe, Mark McKoy, and Dawn Deel (NETL Technology Development and Integration Center), and Darin Damiani (DOE Office of Fossil Energy and Carbon Management) for programmatic guidance, direction, and support.

The authors would like to thank Bryan Tennant and Scott Workman for data collection and technical support. The authors would like to thank the staff of NETL's Geologic Characterization, Analytics and Modeling laboratory for continued operational support.

ABSTRACT

The computed tomography (CT) facilities and the Multi-Sensor Core Logger (MSCL) at the National Energy Technology Laboratory (NETL) in Morgantown, West Virginia were used to characterize the Lower Mt. Simon Sandstone and Eau Claire Formation core from the One Earth Energy Well #1 (OEE Well #1) in the Illinois Basin.

The primary impetus of this work is a collaboration between the U.S. Department of Energy (DOE), the Illinois State Geological Survey (ISGS), the University of Illinois, and One Earth Energy to characterize and make publicly available core information of interest to carbon sequestration efforts in the Illinois Basin. This stratigraphic well and the core data produced in this report will aid in understanding the carbon sequestration potential of the Lower Mt. Simon Sandstone and the sealing capacity of the overlying units. The resultant datasets are presented in this report and can be accessed from NETL's Energy Data eXchange (EDX) online system using the following link: https://edx.netl.doe.gov/dataset/illinois-storage-corridor-one-earth-energy-1-core.

All equipment and techniques used were non-destructive, enabling future examinations and analyses to be performed on these cores. Imaging with the NETL medical CT scanner was performed on the entire core. Qualitative analysis of the medical CT images, coupled with X-ray fluorescence (XRF), P-wave, and magnetic susceptibility measurements from the MSCL were useful in identifying zones of interest for more detailed analysis. The ability to quickly identify key areas for more detailed study with higher resolution will save time and resources in future studies. Targeted higher resolution CT scanning of select sections was performed with NETL's industrial and micro-CT scanners based on the lower resolution imaging and core availability. The combination of methods used provides a multi-scale analysis the core; the resulting macro and micro descriptions are relevant to many subsurface energy related examinations traditionally performed at NETL.

1. INTRODUCTION

Evaluation of reservoir samples can support resource estimations for geologic carbon dioxide (CO_2) injection. While it is common for commercial entities to perform these characterizations, the resources necessary to conduct these analyses are not always available to the broader interest base, such as state agencies and research-based consortiums. To meet the growing need for comprehensive and high-quality lithologic data for collaborative research initiatives, the U.S. Department of Energy's (DOE) National Energy Technology Laboratory (NETL) has used available resources in conjunction with previous techniques and new, innovative methodologies to develop a systematic approach for the evaluation of cores.

In this study, the primary objective was to characterize core from depth with methods not available to most researchers. The data is presented in several formats here and online from NETL's Energy Data eXchange (EDX) (https://edx.netl.doe.gov/dataset/illinois-storage-corridor-one-earth-energy-1-core) that are potentially useful for various analyses. However, little detailed analysis is presented in this report, as the research objective was not to conduct a site characterization, but rather to develop the data for others to utilize and to create a digital representation of the core that could be preserved.

1.1 SITE BACKGROUND

The One Earth Energy Well#1 (OEE Well #1) was drilled in McLean County, Illinois in support of the Illinois Storage Corridor (ISC) CarbonSAFE project (Whittaker, 2022). One Earth Energy, located in Gibson City, in Ford County, Illinois produces CO_2 gas as a byproduct of the manufacturing fuel-grade ethanol and distiller grain, a livestock feed supplement. It is partnering with the Illinois State Geological Survey (ISGS) to study whether the 0.45 $MtCO_2$ it produces annually can be safely injected and permanently sequestered in the underlying Lower Mt. Simon Sandstone. The OEE Well #1 was drilled as part of the Illinois Storage Corridor project, which is funded by the U.S. DOE through the NETL under contract number DE-FE 0031892.

The OEE Well #1 is a stratigraphic characterization well drilled in support of the ISC project, 4 miles west of the One Earth Energy facility, just across the county line in McLean County. Once the project moves into the injection phase, the well will be used for monitoring. The well was completed on 2/12/2022, reaching a total depth of 7,104 ft, and terminating in Precambrian basement rock. Core recovered from the Eau Claire Formation portion of the well (4,310–4,370 ft), and the lowermost Mt. Simon Sandstone and underlying Argenta Formation (6,341–6,521.04 ft) is characterized in this report.

1.2 GEOLOGIC BACKGROUND

The OEE Well #1 was drilled to determine the feasibility of developing commercial scale carbon capture the One Earth Energy ethanol plant, with a primary focus on geological storage in the underlying Mt. Simon Sandstone. The OEE Well #1 site is structurally and tectonically stable, with no deep faults known within a 25-mile radius, and the nearest known major fault located approximately 65 miles to the north of the site (Nelson, 1995).

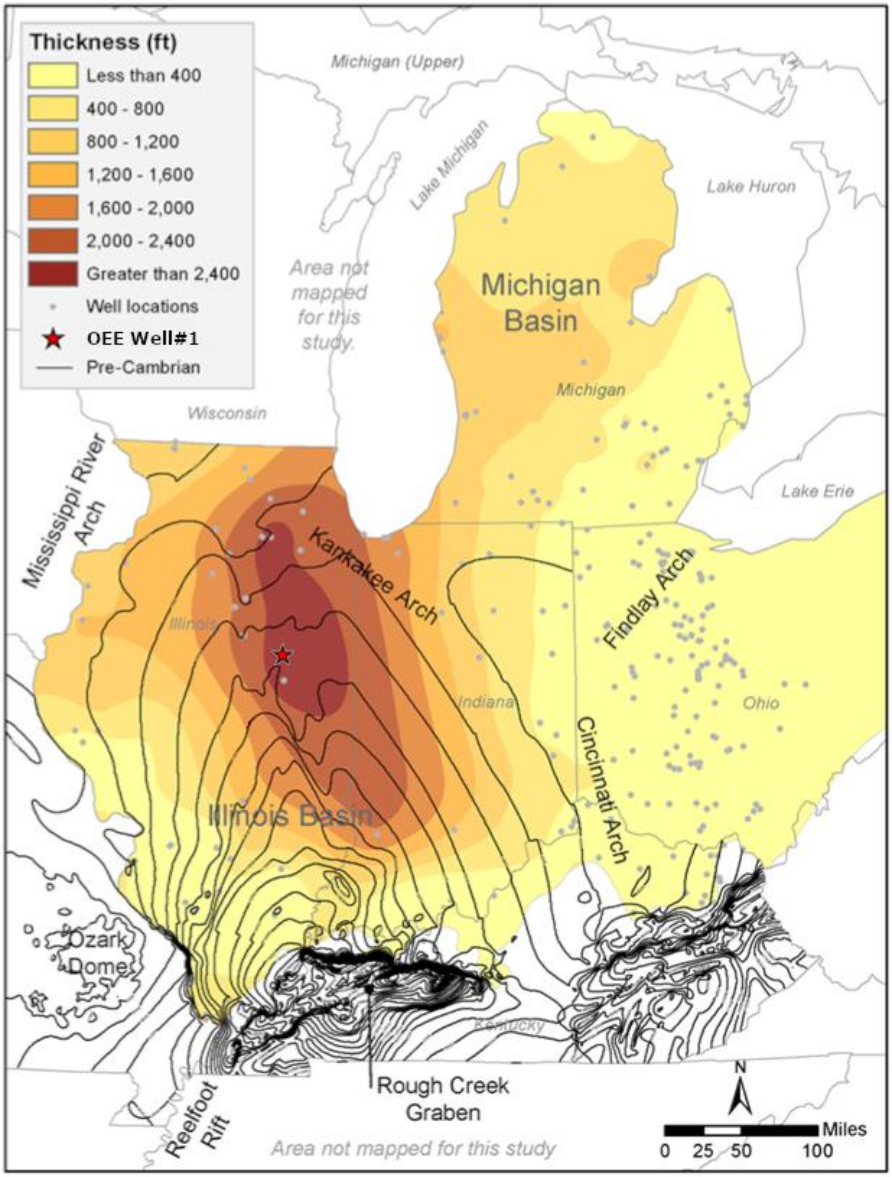

Figure 1: Map of Illinois illustrating the extent and thickness of the Mt. Simon Formation. The red star indicates site location of the OEE Well #1 (Modified from Freiburg et al., 2016).

The One Earth Energy facility and Well #1 location are in the area where the Mt. Simon Sandstone and the targeted zone within it are the thickest (Figure 1 and Figure 2) in the center of the depositional basin in east-central Illinois. Isopach maps of the Mt. Simon (Figure 1) include the underlying Argenta Formation, which was discovered during drilling for the Illinois Basin Decatur Project, and is not a formally recognized formation (Freiburg et al., 2022). It is delineated as a unit based on its medium to very coarse-grained, sometimes conglomeratic sandstone lithology, and is presumed to be related to local rifting. During drilling, the top of the Mt. Simon Sandstone was encountered at 4,455 ft below mean sea level and the formation had a total thickness of about 2,463 ft including the Argenta. Based on studies of the Mt. Simon from the western flanks of the Mt. Simon depocenter, the lower Mt. Simon is generally more porous

than its upper members (Freiburg et al., 2016) and is generally made up of shallow marine, fluvial, and eolian deposits (Reesink et al., 2020) compared to the tidal to subtidal depositional environment in the upper (Friedburg et al., 2014). Moving up section from the lower Mt. Simon, finer grains and quartz cementation are typically prevalent and generally create poorer reservoir properties in the middle Mt. Simon. Better reservoir conditions are therefore expected in the lower Mt. Simon (Korose and Whittaker, 2020; Morse and Leetaru, 2005). The lower Mt. Simon Sandstone as characterized in other wells in the area, is made up of thick-bedded, medium to coarse-grained, cross-bedded arkosic sandstone beds interbedded with thin intervals of fine-grained sandstone to mudstone (Morse and Leetaru, 2005; Friedburg et al., 2014). This "Arkosic zone" is the target for Mt. Simon core collection at the One Earth Energy CarbonSAFE site and exhibits an average porosity of 14.4% in the retrieved core. The characterized core includes 128 ft of the Arkosic zone, as well as 52 ft of the underlying Argenta Formation.

The Eau Claire Formation is the primary sealing formation regionally, as well as at the OEE Well #1 site, and occurs at a depth of 3,921 ft in OEE Well #1, with a total thickness of 534 ft. It is subdivided into a basal Elmhurst Sandstone member, which has a gradational boundary with the Mt. Simon, and the Eau Claire shale, the principal sealing unit. Retrieved core between 4,310 and 4,368 ft is from this specific sealing shale unit.

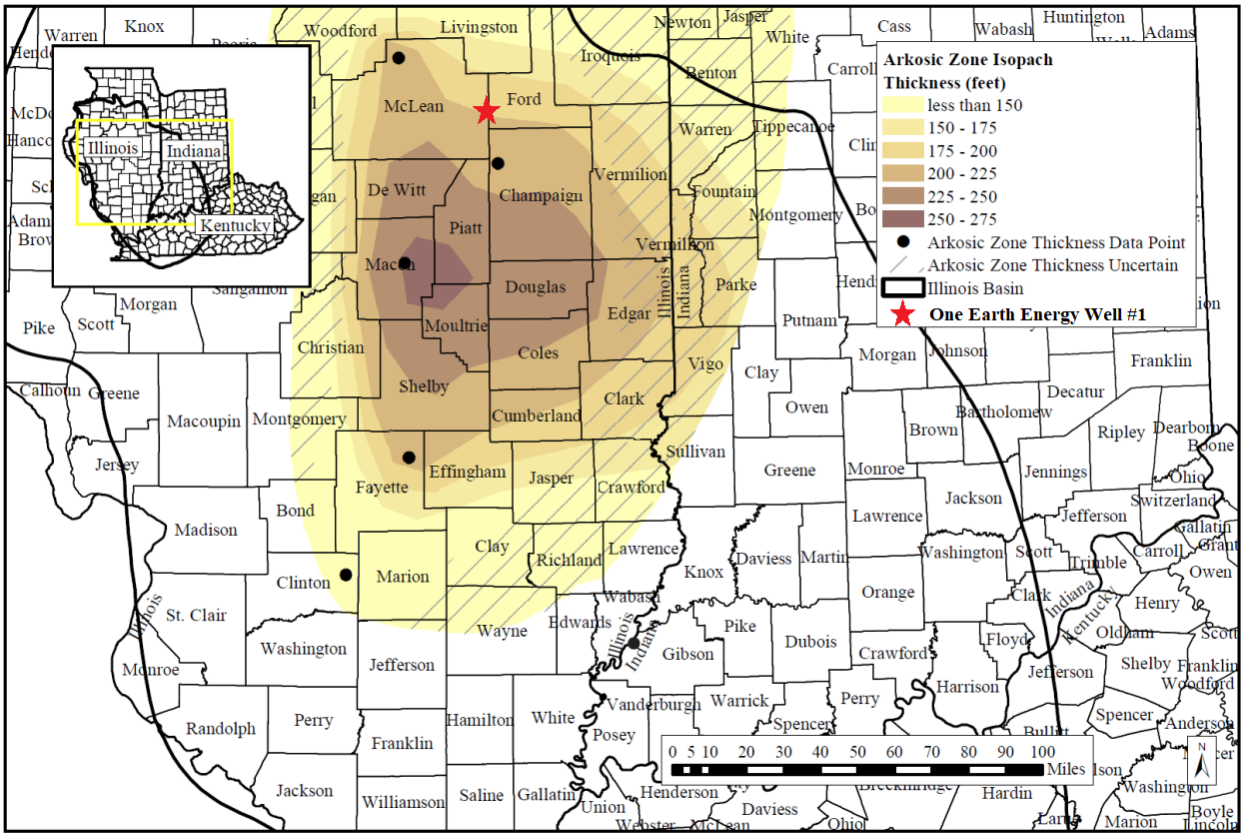

Figure 2: Isopach map of Arkosic Zone in the Lower Mt. Simon Sandstone, with OEE Well #1 site marked with red star. (Modified from Blakley et al., 2019).

2. CORE PHOTOGRAPHS

Core photographs of the Mt. Simon and Argenta core (6,360 to 6,521.5 ft depth) are presented to complement the CT imaging and core logging. At the time of this publication the photographs of the Eau Claire are unavailable, however they will be added to the EDX data at a later date.

OEE Well #1:

6,340–6,350 ft

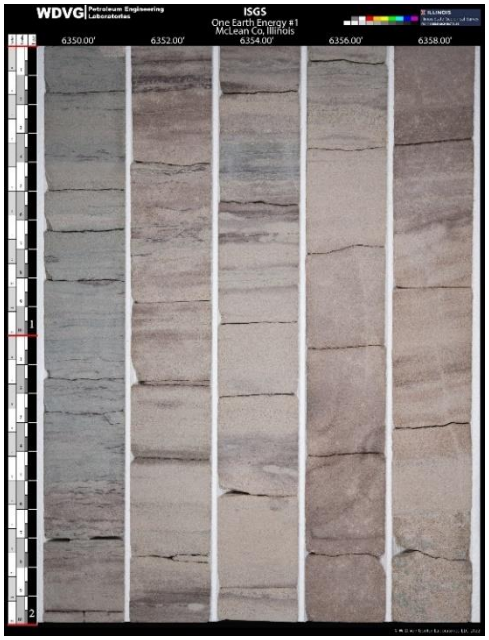

6,350–6,360 ft

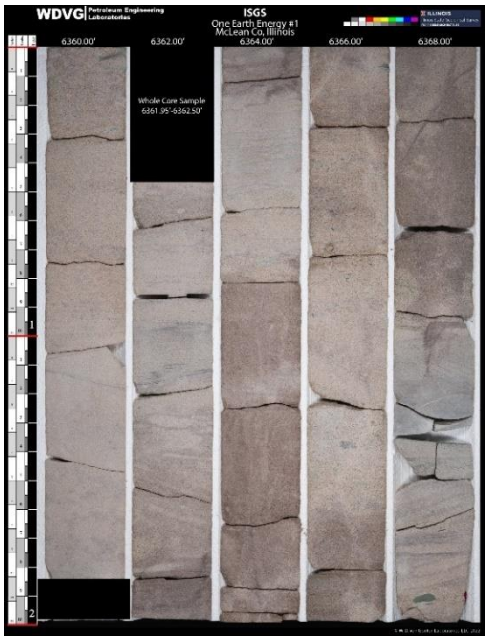

6,360–6,370 ft

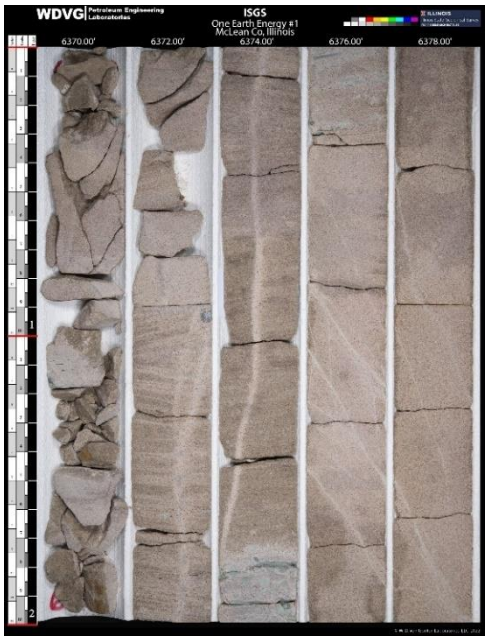

6,370–6,380 ft

Figure 3: Photographs of the OEE Well #1 from 6,340–6,380 ft.

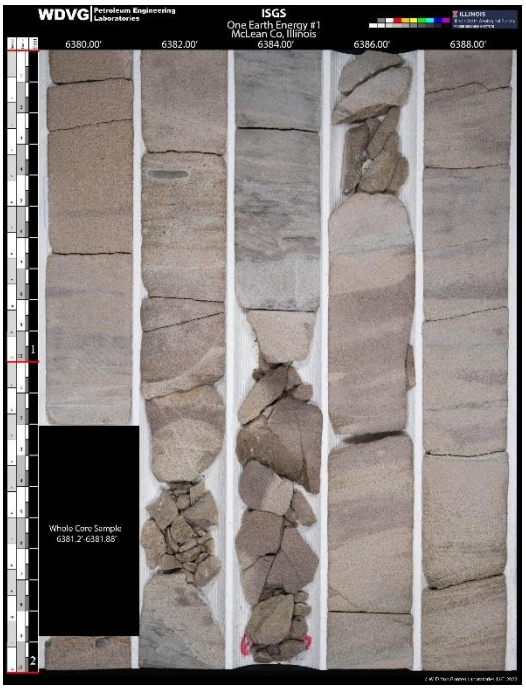

6,380–6,390 ft

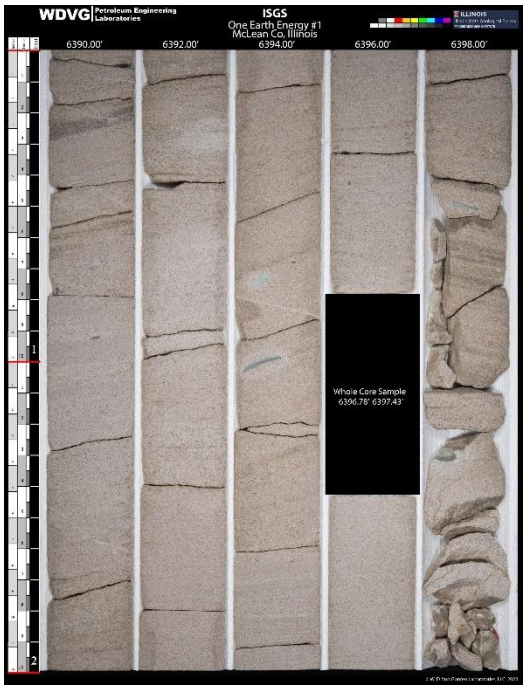

6,390–6,400 ft

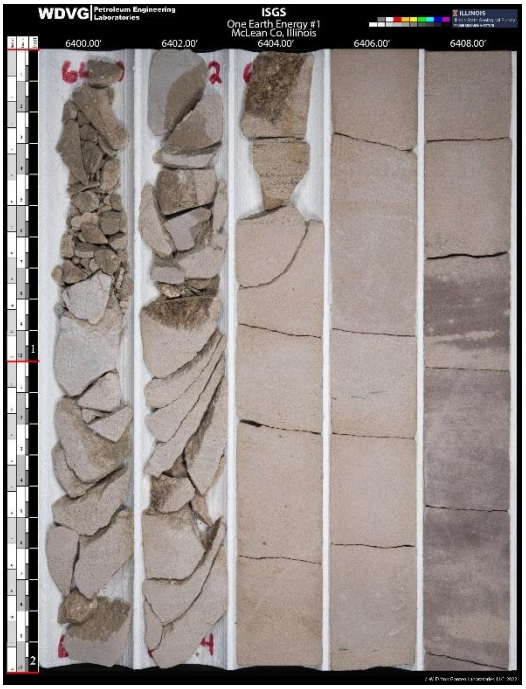

6,400–6,410 ft

6,410–6,420 ft

Figure 4: Photographs of the OEE Well #1 from 6,380–6,420 ft.

6,420–6,430 ft

6,430–6,430.5 ft

6,431–6,441 ft

6,441–6,451 ft

Figure 5: Photographs of the OEE Well #1 from 6,420–6,451 ft.

6,451–6,461 ft

6,461–6,471 ft

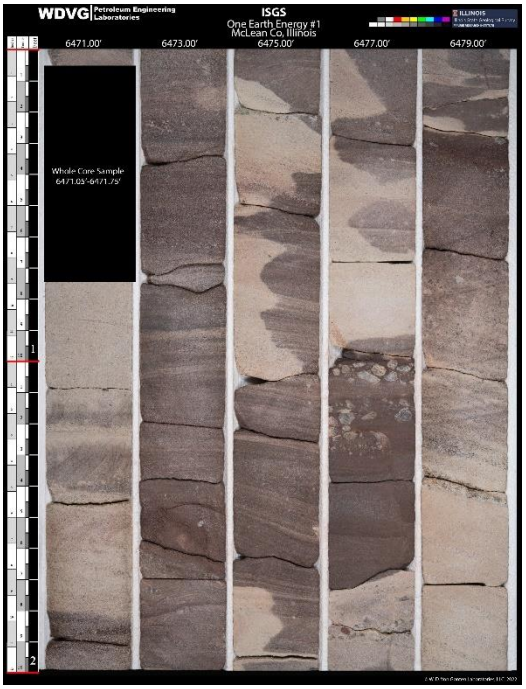

6,471–6,481 ft

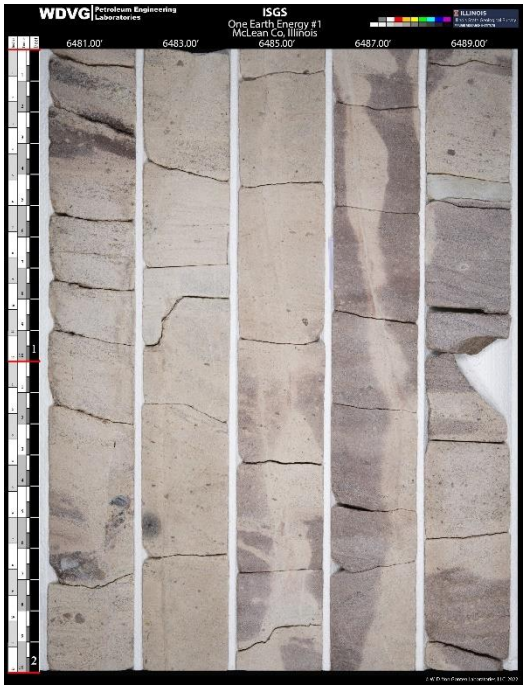

6,481–6,491 ft

Figure 6: Photographs of the OEE Well #1 from 6,451–6,491 ft.

6,491–6,501 ft

6,501–6,511 ft

6,511–6,521 ft

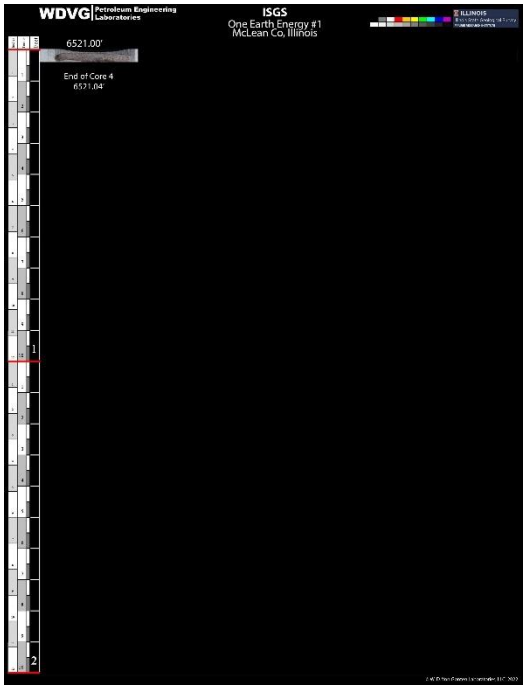

6,521–6,521.5 ft

Figure 7: Photographs of the OEE Well #1 from 6,491–6,521.5 ft.

3. DATA ACQUISITION AND METHODOLOGY

The core was evaluated using computed tomography (CT) scanning and multi-sensor core logging including X-ray fluorescence (XRF) spectrometry.

3.1 MEDICAL CT SCANNING

Core scale CT scanning was done with a Toshiba® Aquilion TSX-101A/R medical scanner as shown in Figure 8. The medical CT scanner generates images with a resolution in the millimeter range, with scans having voxel resolutions of 0.43 x 0.43 mm in the XY plane and 0.50 mm along the core axis. The scans were conducted at a voltage of 135 kV and at a current of 200 mA. Subsequent processing and combining of stacks were performed to create three-dimensional (3D) volumetric representations of the cores and a two-dimensional (2D) cross-section through the middle of the core samples using ImageJ (Rasband, 2018). The variation in greyscale values observed in the CT images indicates changes in the CT number obtained from the CT scans, which is directly proportional to changes in the attenuation and density of the scanned rock. Darker regions are less dense. As can be seen in Figure 12 through Figure 33, filled fractures, open fractures, and changes in bedding structure can all be resolved via careful examination of the CT images. While the medical CT scanner was not used for detailed characterization in this study, it allowed for non-destructive bulk characterization of the core.

Figure 8: Toshiba® Aquilion™ Multislice Helical CT Scanner at the NETL used for core analysis.

3.2 INDUSTRIAL CT SCANNING

High resolution CT scans were performed on intervals of interest using the North Star Imagining Inc. M-5000® Industrial CT Scanner shown in Figure 9. The system is used to obtain higher resolution scans, resolving some unclear features from the medical scans.

The scans were performed at varying voltages and currents to provide a balance between resolution and a sufficient sample penetration for each sample. Scans consisted of 1,440 radiographs, or at every 0.25°; radiographs were comprised of 10 images averaged with a 5 second acquisition for each image to ensure sufficient image contrast. Representative images of these scans can be seen in Figure 35 and Figure 36. Full resolution and scaled datasets are available on EDX for further analyses.

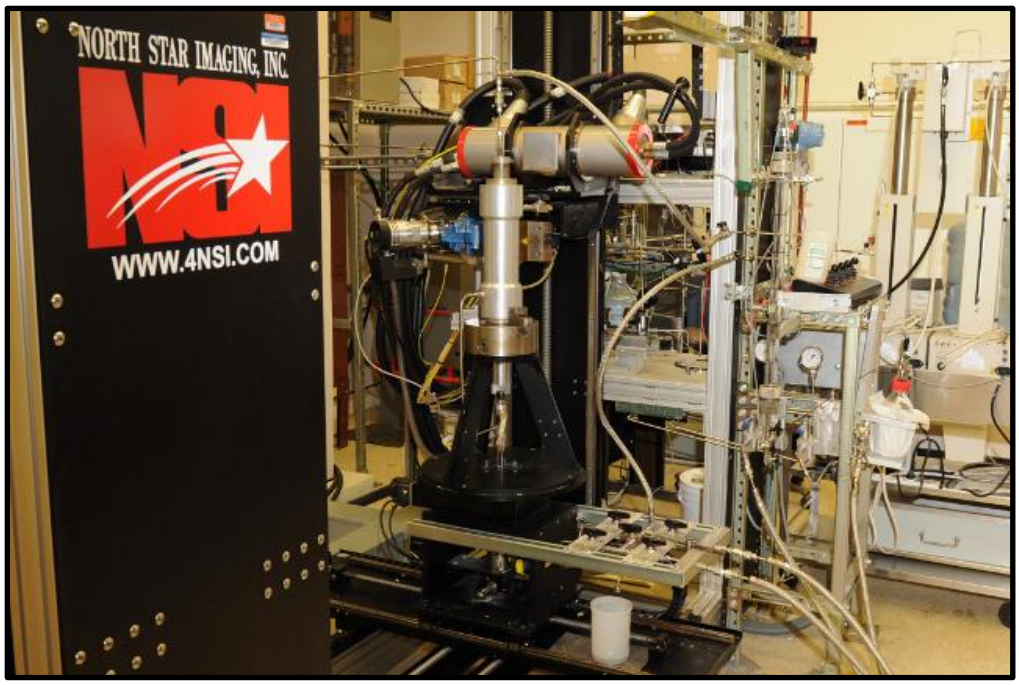

Figure 9: North Star Imaging Inc. M-5000 ® Industrial CT Scanner at NETL used for core analysis.

3.3 MICRO-CT SCANNING

Micro-CT scanning was performed using two scanners, a Zeiss Xradia MicroXCT-*400* (Xradia) scanner and a Tescan DynaTOM micro-CT scanner. The Xradia system has the highest resolution of the scanners at NETL and scans samples sized from sub-mm to 25 mm. The DynaTOM performs both dynamic and static imaging and can scan both sub-mm to cm-scale samples (Figure 10). Both scanners provide detailed image data that can be used to infer porosity, mineralogy, and structure.

Representative images of the data from the Xradia scanner can be viewed in Figure 41 through Figure 51. Full resolution and scaled data sets are available on EDX for further analyses.

Figure 10: Tescan DynaTOM micro-CT scanner used for high-resolution CT images at NETL used for core analysis.

3.4 CORE LOGGING

Geophysical measurements of P-wave travel time, magnetic susceptibility, and attenuated gamma counts were obtained with a Geotek® Multi-Sensor Core Logging system on competent sections of the core (Figure 52 and Figure 53). Additionally, the system was used to measure bulk elemental chemistry with a built-in, portable XRF spectrometer.

The compiled core logs were scaled to fit on single pages for rapid review of the combined data from the medical CT scans and XRF readings. Core scale CT scanning was done with a medical Toshiba® Aquilion TSX-101A/R medical CT scanner.

3.4.1 Magnetic Susceptibility

Magnetic susceptibility is a measure of the degree of magnetization in a sample. The sample is exposed to an external magnetic field and magnetic susceptibility is the measured magnetic response to that field:

$$J = kH$$

Where, J is the magnetic response (per unit volume), k is volume susceptibility, and H is an external magnetic field. The measurement unit is dimensionless (abbreviated as SI). Positive magnetic susceptibility indicates that materials are paramagnetic and occurs in rocks that are majority ferromagnetic, ferrimagnetic, or antimagnetic (iron bearing) materials. Negative magnetic susceptibility indicates that materials are diamagnetic and occurs in rocks dominated by non-iron material (i.e., calcite or quartz). Table 1 lists examples of common magnetic susceptibility ranges (Hunts et al., 1995).

Magnetic susceptibility is measured using the Bartington point sensor, where a 1-cm diameter, low intensity (8.0 A/m RMS), non-sensitive, alternating magnetic field (2 kHz) is generated for 10 seconds. To minimize any potential drift in the oscillating field the point sensor is zeroed at the beginning and end of the sample, as well as, after every fifth measurement. The point sensor due to the small field, is limited in whole core measurements, and additionally is temperature dependent (Geotek Ltd. Multi-Sensor Core Logger Manual, Version 05-10, 2010).

Table 1: Magnetic Susceptibility Values for Common Minerals (Hunts et al., 1995)

Mineral	X (*10^{-6}) SI
Water	9
Calcite	-7.5 to -39
Halite, Gypsum	-10 to -60
Illite, Montmorillonite	330 to 410
Pyrite	5 to 3,500
Haematite	500 to 40,000
Magnetite	1,000,000 to 5,700,000

3.4.2 P-wave Velocity

P-wave velocity measurements are performed to measure the acoustic impedance of a geologic sample with compressional waves. Acoustic impedance is a measure of how well a material transmits vibrations, which is directly proportional to density and material consolidation. An example of a material that has a low acoustic impedance would be air, with a wave speed of 330 m/s, whereas granite would have high acoustic impedance, with a wave speed of >5,000 m/s. These measurements can be proxies for seismic reflection coefficients and can be translated to field use when doing seismic surveys.

The software associated with the Multi-Sensor Core Logger (MSCL) measures the travel time of the pulse with a resolution of 50 ns. The absolute accuracy of the instrument measurements is $\pm$ 3 m/s with a resolution of 1.5 m/s (Geotek Ltd. Multi-Sensor Core Logger Manual, Version 05-10; Geotek Ltd., 2010).

3.4.3 Gamma Density

Gamma density is acquired by subjecting the sample to gamma radiation and then measuring the attenuation of that radiation. The attenuation is directly proportional to the density of the sample and is acquired by measuring the difference between radiation energy at the emission source and after it passes through the sample. Specifically, the MSCL software calculates the bulk density, ρ, by using the following equation:

$$\rho = \left(\frac{1}{\mu d}\right) \ln\left(\frac{I_o}{I}\right)$$

Where μ is the Compton attenuation coefficient, d is the sample thickness, I_o is the source intensity, and I is the measured intensity.

3.5 XRF SPECTROMETRY

In addition to the geophysical measurements, two portable handheld devices: the Innov-X® XRF Spectrometer and The Olympus Vanta M Series XRF Spectrometer were used to measure relative elemental abundances of aggregated "light elements" up to and including sodium, and various "heavy elements" which were measured individually (Figure 52). Elemental abundances are reported in ppm relative to the total elemental composition (i.e., the total XRF counts).

The XRF spectrometer measures elemental abundances by subjecting the sample to X-ray photons. The high energy of the photons displaces inner orbital electrons in the respective elements. The vacancies in the lower orbitals cause outer orbital electrons to "fall" into lower orbits to satisfy the disturbed electron configuration. The substitution into lower orbitals causes a release of a secondary X-ray photon, which has an energy associated with a specific element. These relative and element-specific energy emissions can then be used to determine bulk elemental composition.

The Innov-X® XRF Spectrometer used a "Mining-Plus Suite" which was run at 6 cm resolution for 120 s exposure time analysis (60 s per beam). The Mining-Plus Suite utilizes a two-beam analysis that resolves major (Mg, Al, Si, P, S, Cl, Fe, K, Ca, and Ti), minor (V, Cu, Ni, Cr, Mn, and Pb), and trace elements (Co, Zn, As, Zr, Mo, Ag, Cd, Sn, Sb, Hf, W, and Bi). The system also resolves an aggregated "light element" (H to Na).

The Olympus Vanta M Series XRF Spectrometer used a "GeoChem (three-beam) Mode" which was run at 30.48 cm (1 ft) resolution for 120 s exposure time analysis (40 s per beam). The GeoChem (three-beam) Mode utilizes a three-beam analysis that resolves major (Mg, Al, Si, P, S, Fe, K, Ca, and Ti), minor (V, Cu, Ni, Cr, Mn, Ba, Sr, and Pb), and trace elements (Co, Zn, As, Zr, Mo, Ag, Cd, Sn, Sb, Hf, W, Th, U, and Bi) and some rare earth elements (Y, Ce, La, Pr, and Nd). The system also resolves an aggregated "light element" (H to Na).

3.6 DATA COMPILATION

Strater® by Golden Software® was used to compile the medical CT data into a series of logs. The data used to generate these logs can be accessed from NETL's EDX online system using the following link: https://edx.netl.doe.gov/dataset/illinois-storage-corridor-one-earth-energy-1-core.

4. RESULTS

Processed 2D slices of the medical CT scans through the cores are shown in this section in Figure 12 to Figure 33.

4.1 MEDICAL CT SCANS

As was discussed previously, the variation in greyscale values observed in the medical CT images indicates changes in the CT number obtained, which is directly proportional to changes in the attenuation and density of the scanned rock (i.e., darker regions are less dense). The images shown in the following section have minimum and maximum greyscale values of 750 and 3,250 in a 16-bit range. The images on EDX contain the full range of 16-bit greyscale values and can be modified to isolate features of interest.

4.1.1 XZ Planes

A 2D image through the center of each core can be found in Figure 12 through Figure 33. These are referred to as XZ planes with the coordinates that are shown in Figure 11. There is a red 2 cm scale bar shown in these images; the retrieved core has a diameter of 3.5 in. (8.89 cm) for reference. The labels below each 2D XZ plane in Figure 12 through Figure 33 are the depth range of each boxed core section; the full range of core lengths shown in each figure is listed in the figure captions. The greyscale range was maintained for all core CT images.

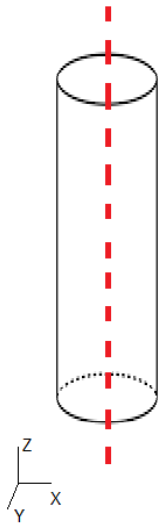

Figure 11: Schematic of the XZ isolated plane through the vertical center of the medical CT scans.

OEE Well #1:

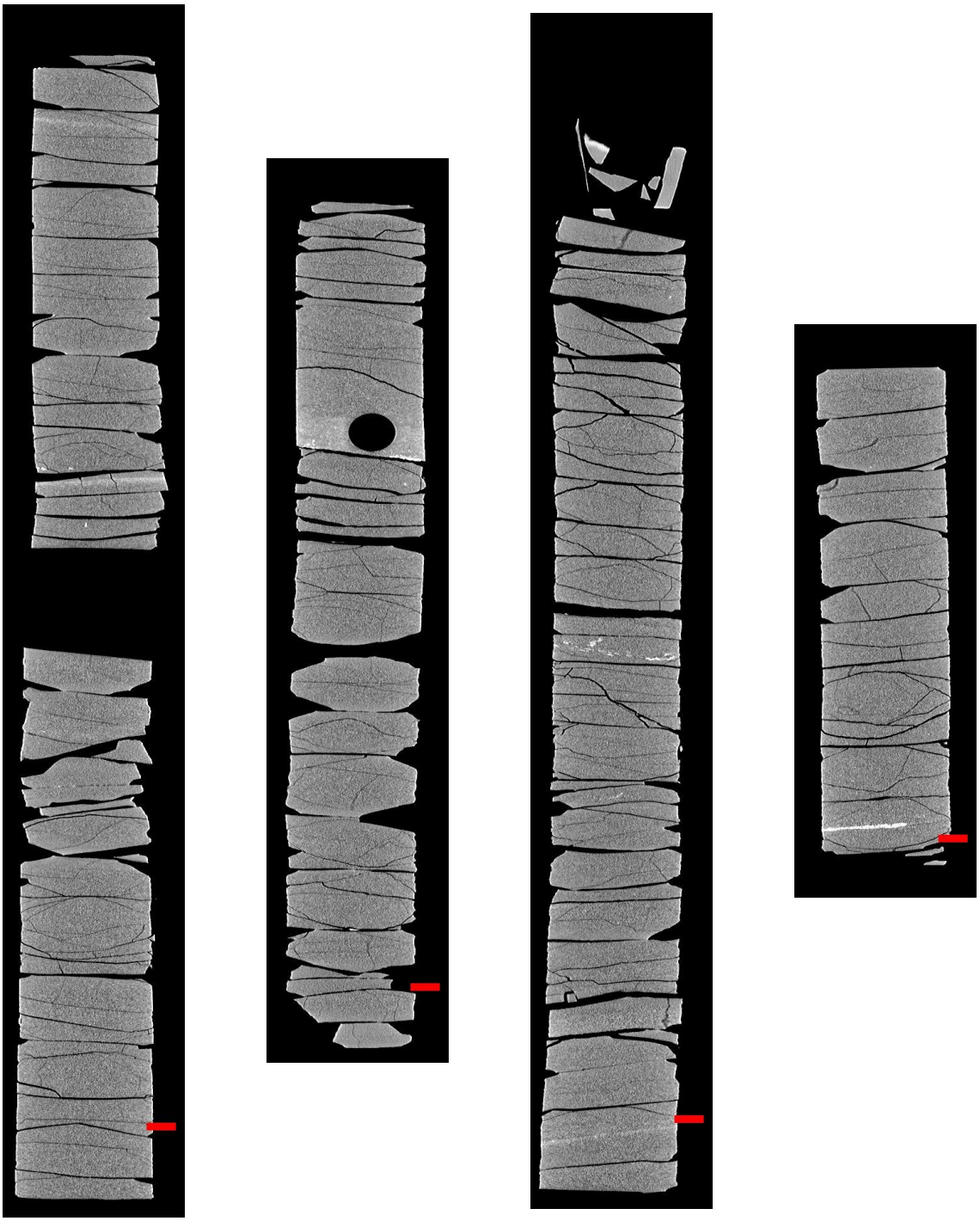

4,310–4,313 ft **4,313–4,316 ft** **4,316–4,319 ft** **4,319–4,320 ft**

Figure 12: 2D midplanes of the medical CT scans of the OEE Well #1 from 4,310–4,320 ft.

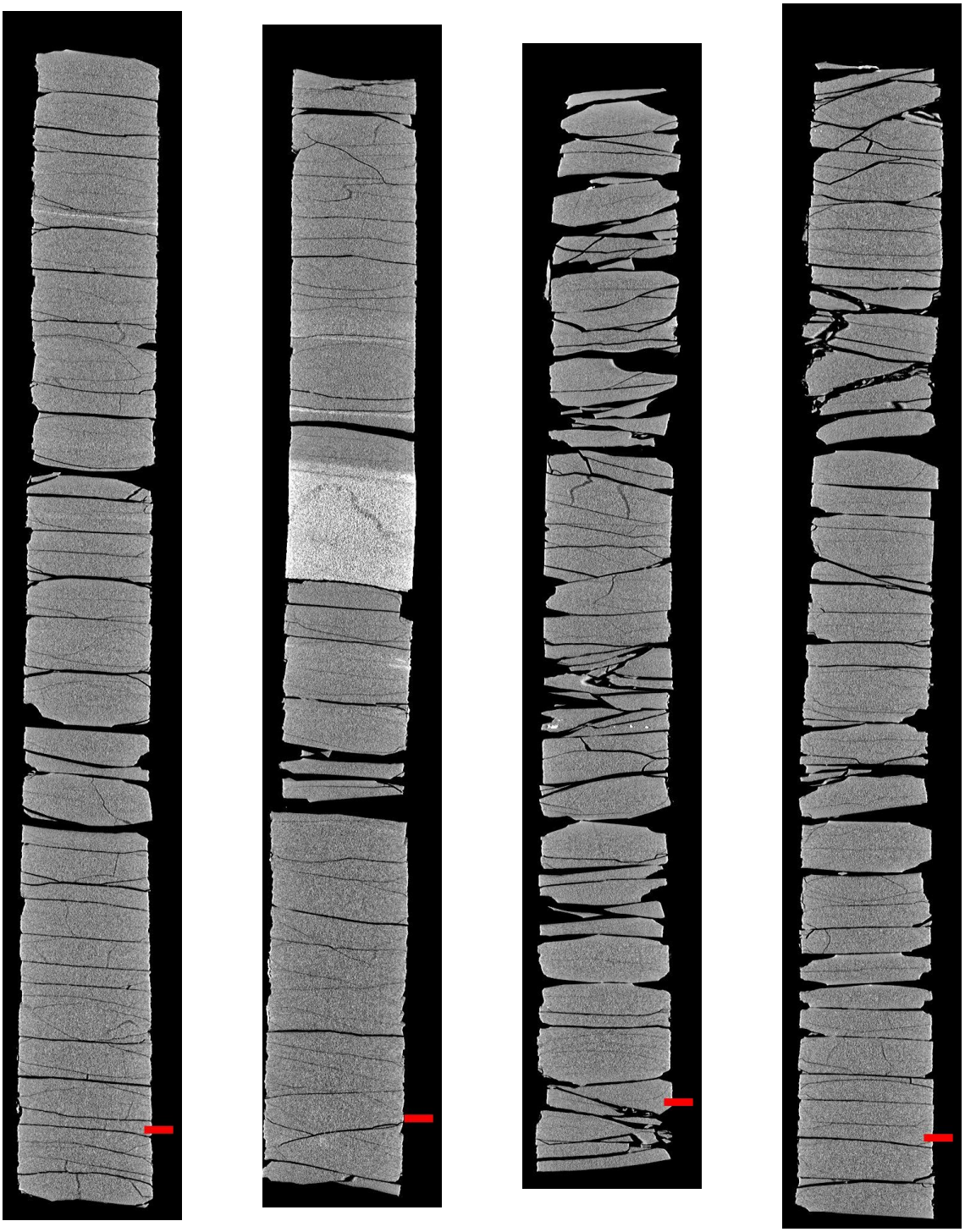

4,320–4,323 ft **4,323–4,326 ft** **4,326–4,329 ft** **4,329–4,332 ft**

Figure 13: 2D midplanes of the medical CT scans of the OEE Well #1 from 4,320–4,332 ft.

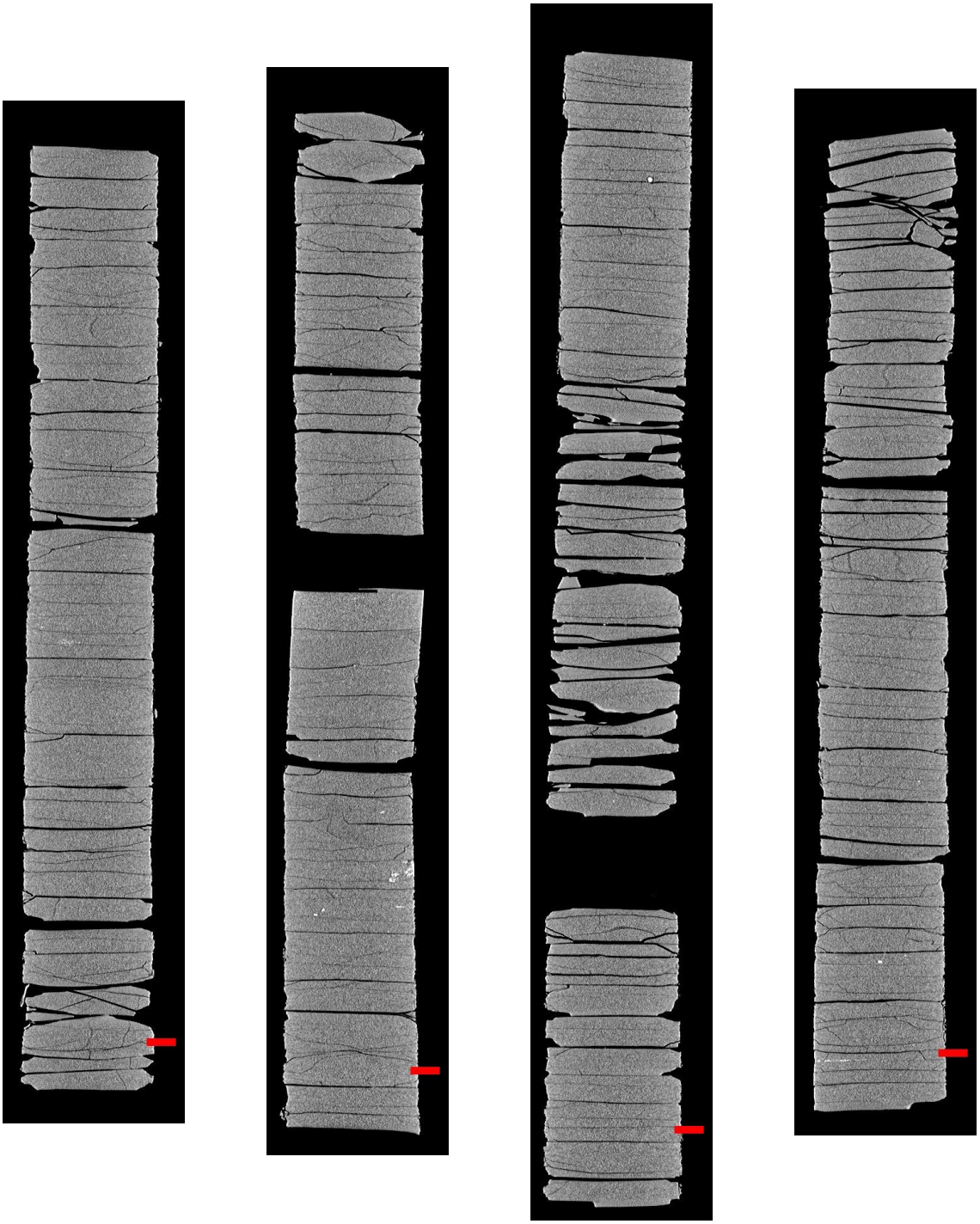

4,332–4,334 ft **4,334–4,337 ft** **4,337–4,340 ft** **4,340–4,343 ft**

Figure 14: 2D midplanes of the medical CT scans of the OEE Well #1 from 4,332–4,343 ft.

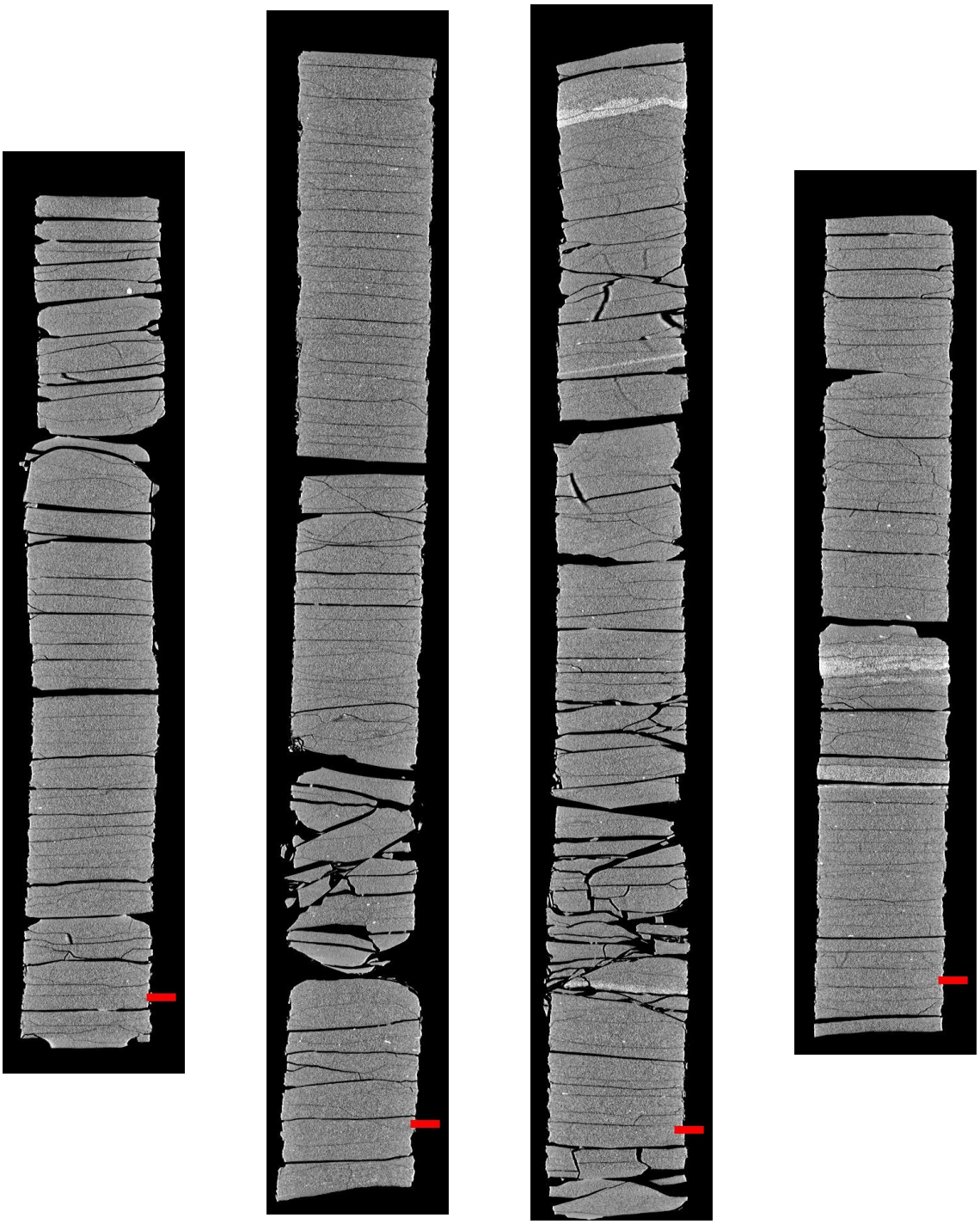

4,343–4,346 ft **4,346–4,348 ft** **4,348–4,351 ft** **4,351–4,353 ft**

Figure 15: 2D midplanes of the medical CT scans of the OEE Well #1 from 4,343–4,353 ft.

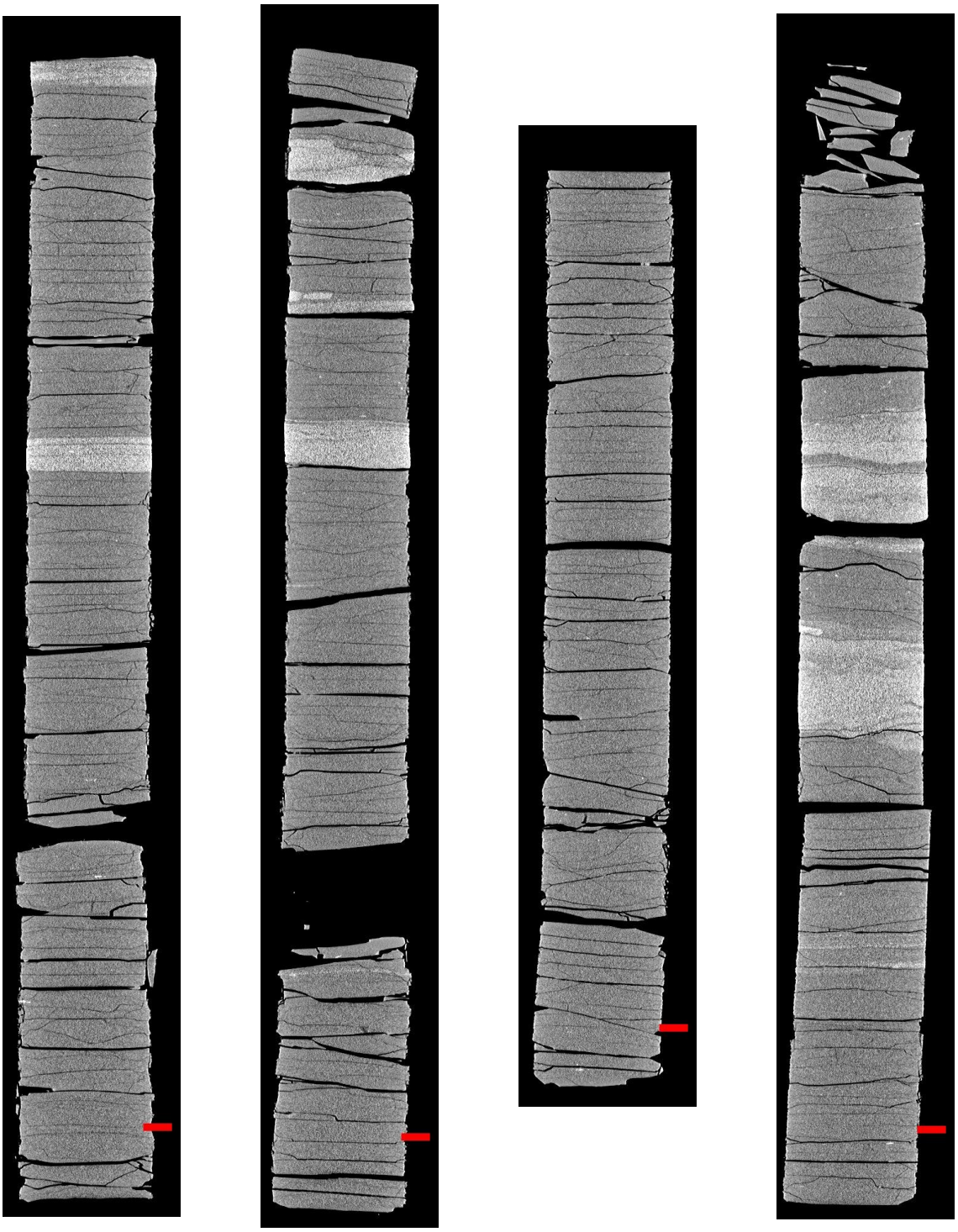

4,353–4,356 ft **4,356–4,359 ft** **4,359–4,361 ft** **4,361–4,364 ft**

Figure 16: 2D midplanes of the medical CT scans of the OEE Well #1 from 4,353–4,364 ft.

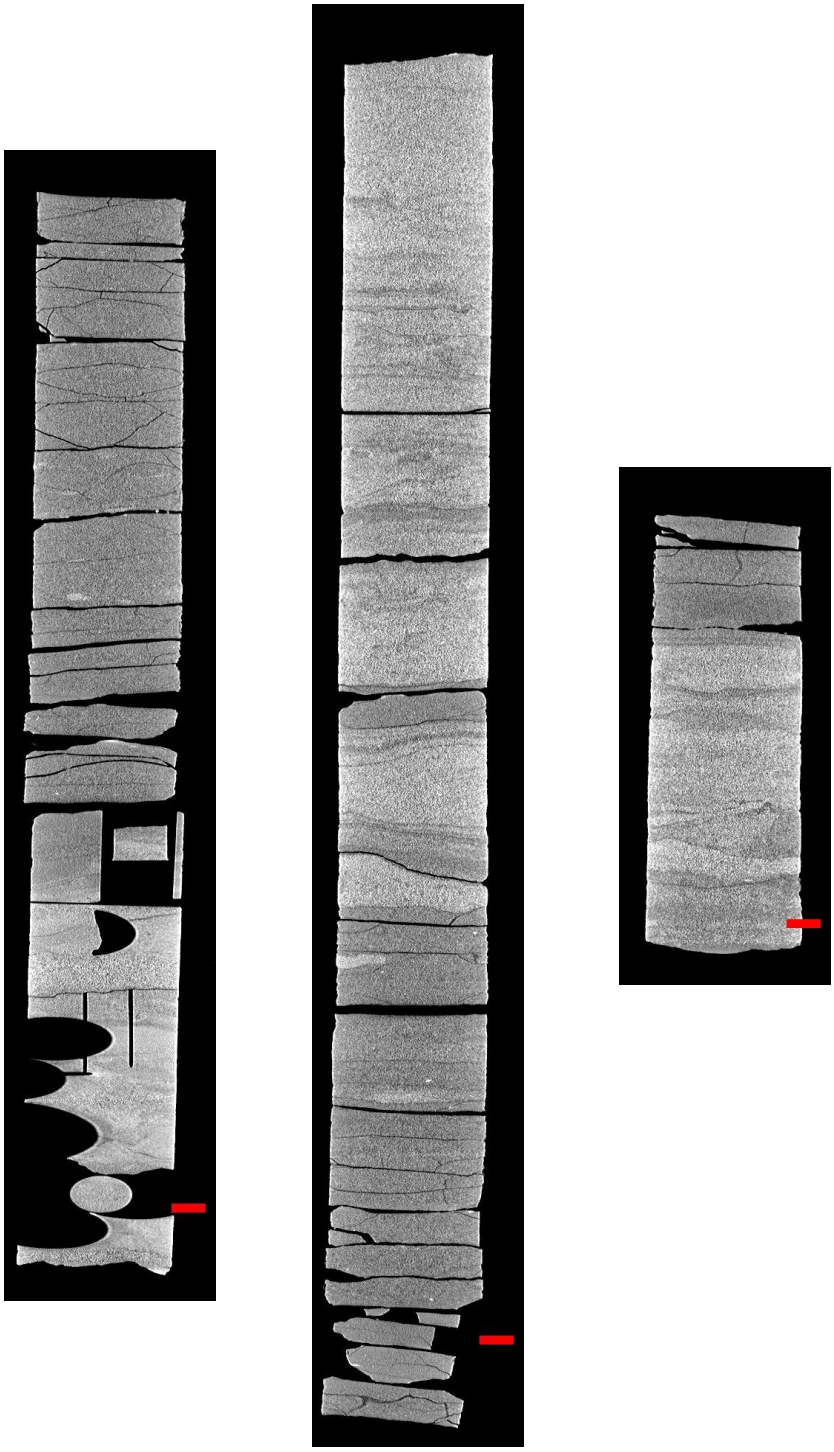

4,364–4,367 ft **4,367–4,370 ft** **4,370–4,371 ft**

Figure 17: 2D midplanes of the medical CT scans of the OEE Well #1 from 4,364–4,371 ft.

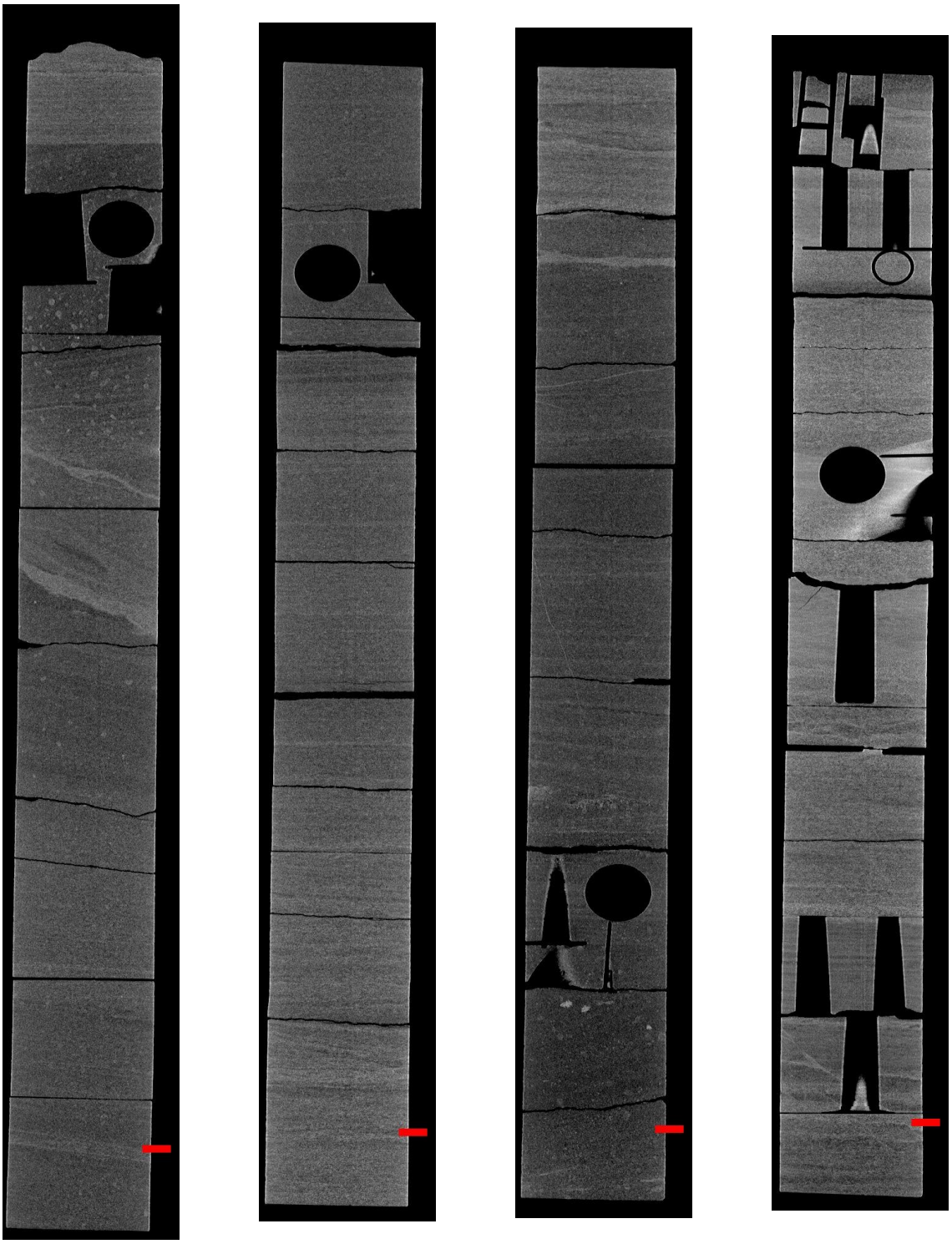

6,341–6,344 ft **6,344–6,347 ft** **6,347–6,350 ft** **6,350–6,353 ft**

Figure 18: 2D midplanes of the medical CT scans of the OEE Well #1 from 6,341–6,353 ft.

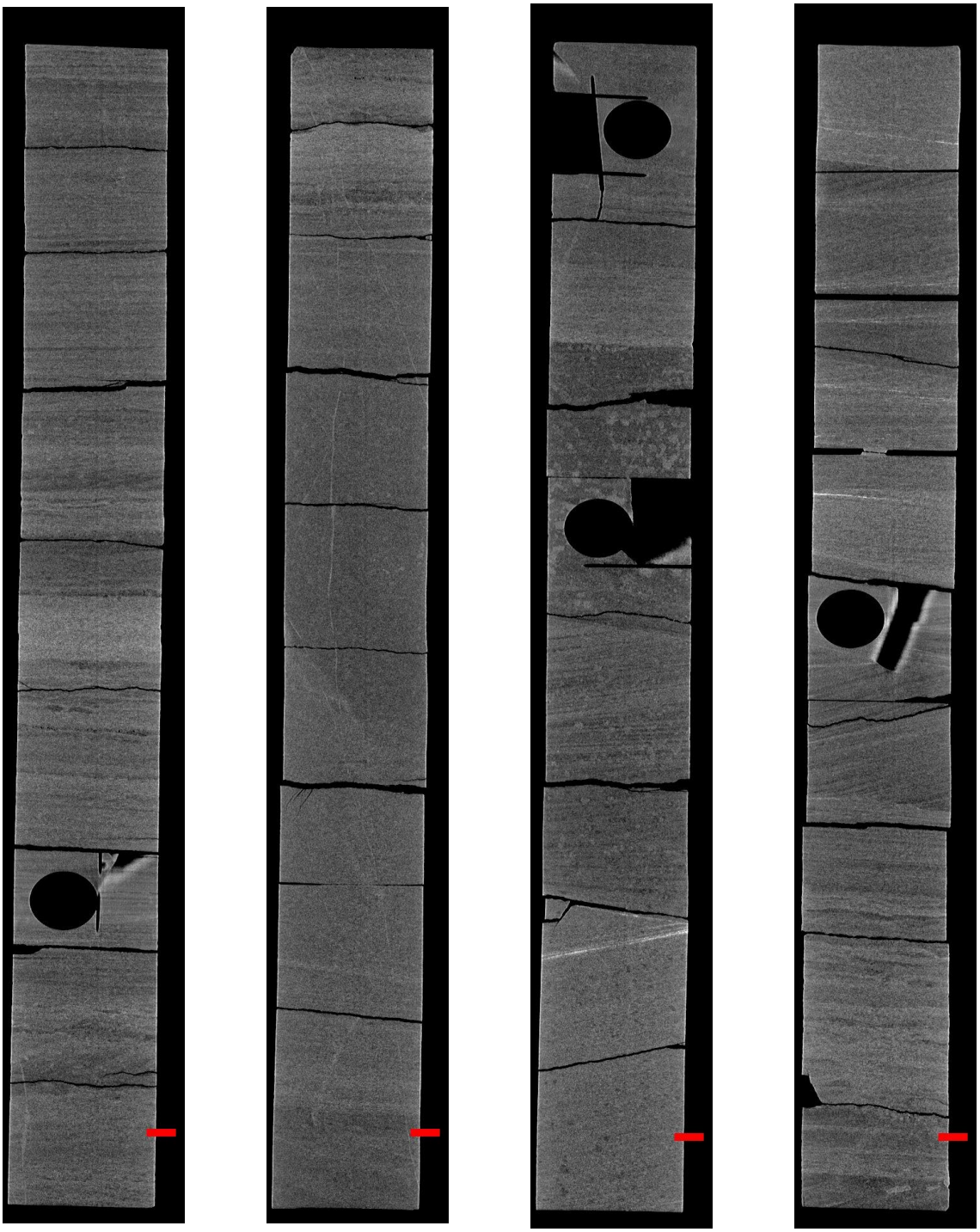

6,353–6,356 ft **6,356–6,359 ft** **6,359–6,362 ft** **6,362–6,365 ft**

Figure 19: 2D midplanes of the medical CT scans of the OEE Well #1 from 6,353–6,365 ft.

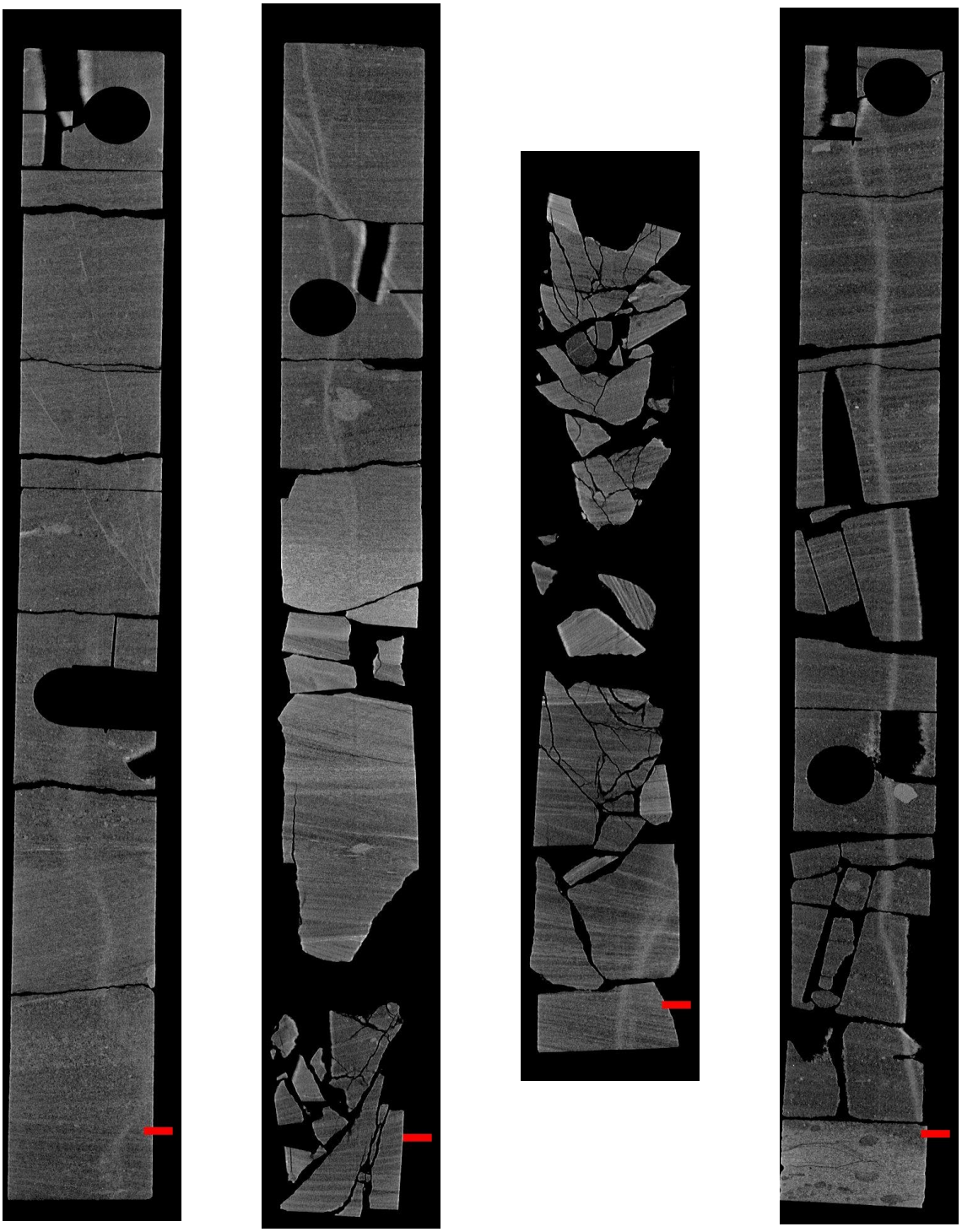

6,365–6,368 ft **6,368–6,370 ft** **6,370–6,373 ft** **6,373–6,376 ft**

Figure 20: 2D midplanes of the medical CT scans of the OEE Well #1 from 6,365–6,376 ft.

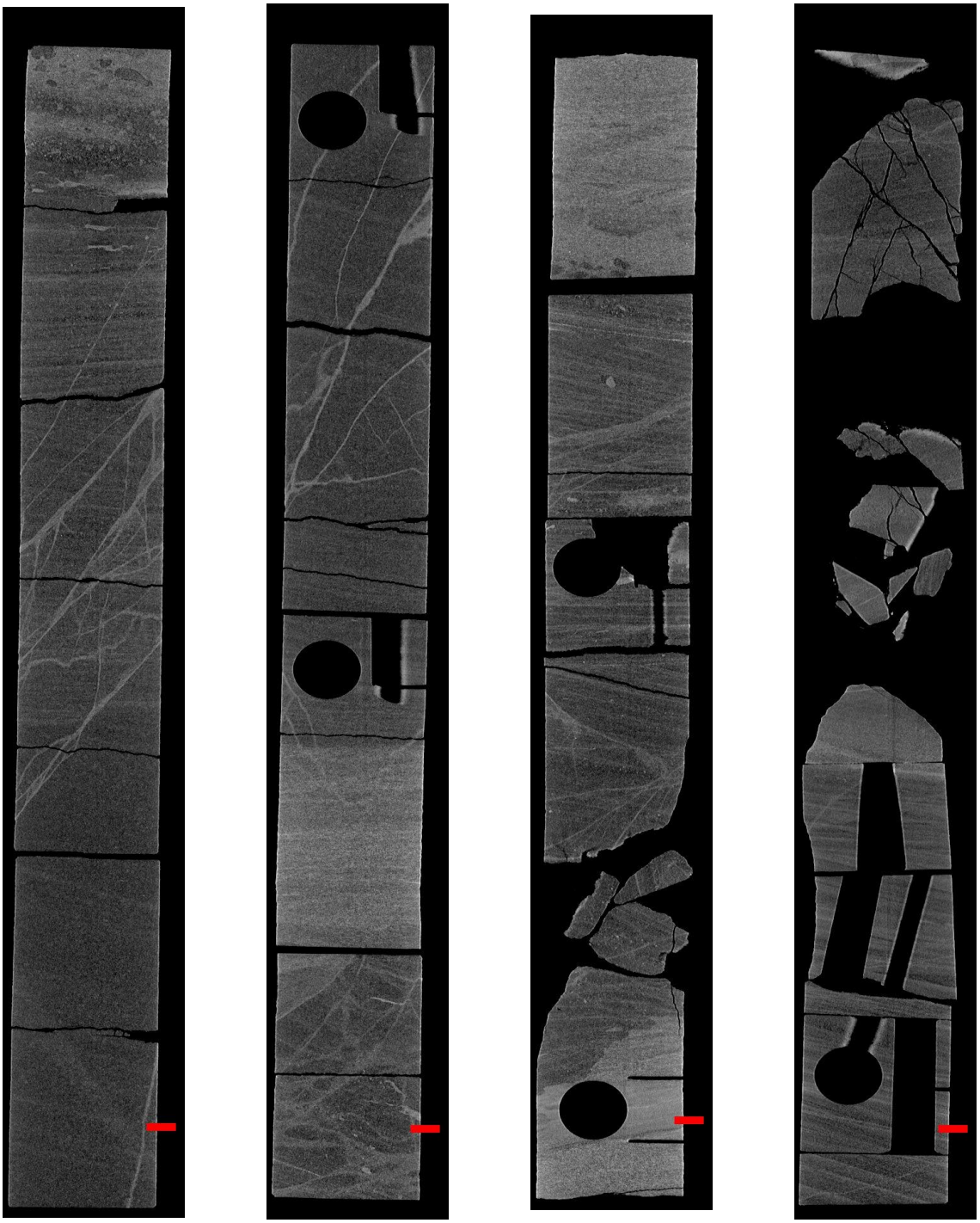

6,376–6,379 ft **6,379–6,382 ft** **6,382–6,385 ft** **6,385–6,388 ft**

Figure 21: 2D midplanes of the medical CT scans of the OEE Well #1 from 6,376–6,388 ft.

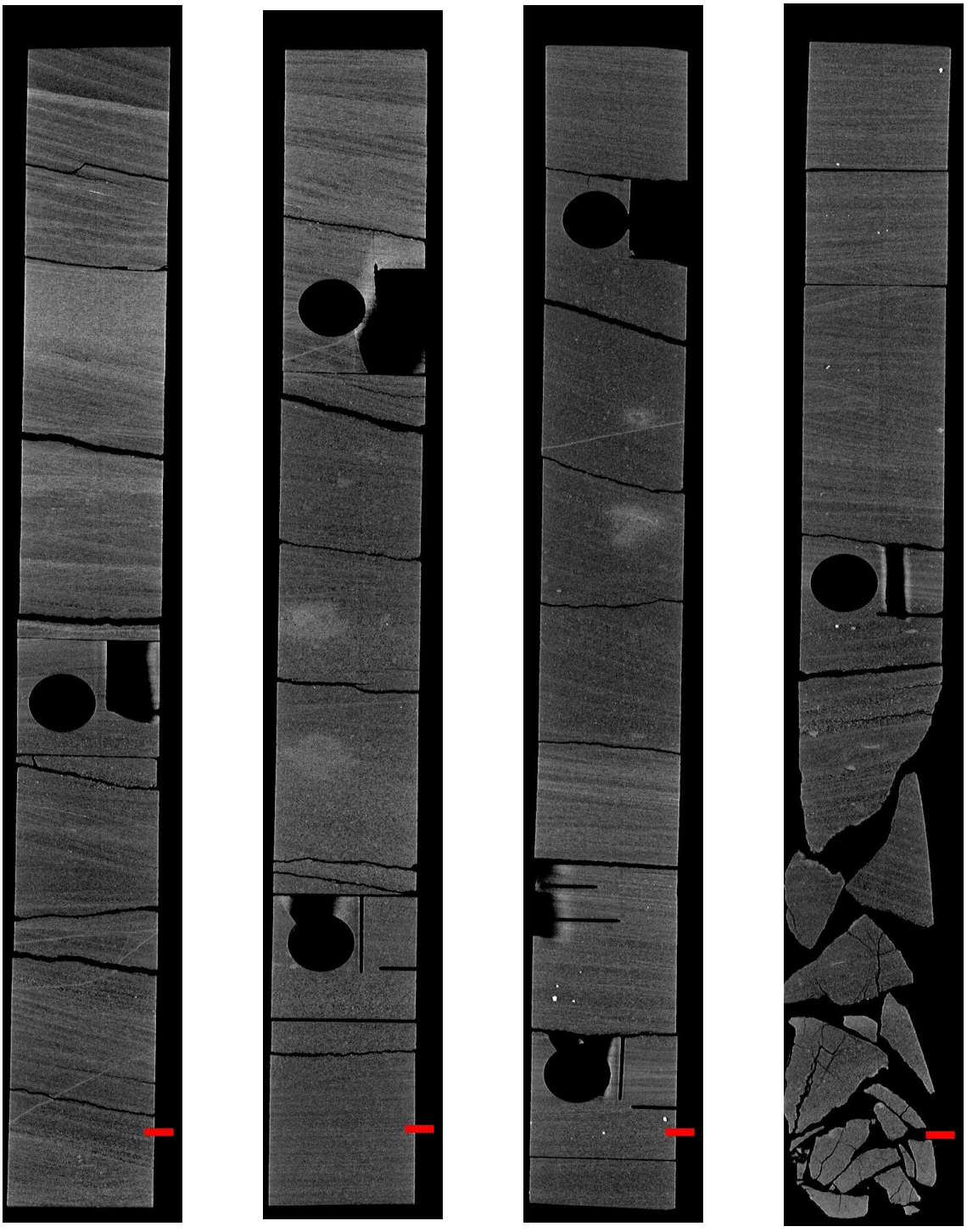

6,388–6,391 ft **6,391–6,394 ft** **6,394–6,397 ft** **6,397–6,400 ft**

Figure 22: 2D midplanes of the medical CT scans of the OEE Well #1 from 6,388–6,400 ft.

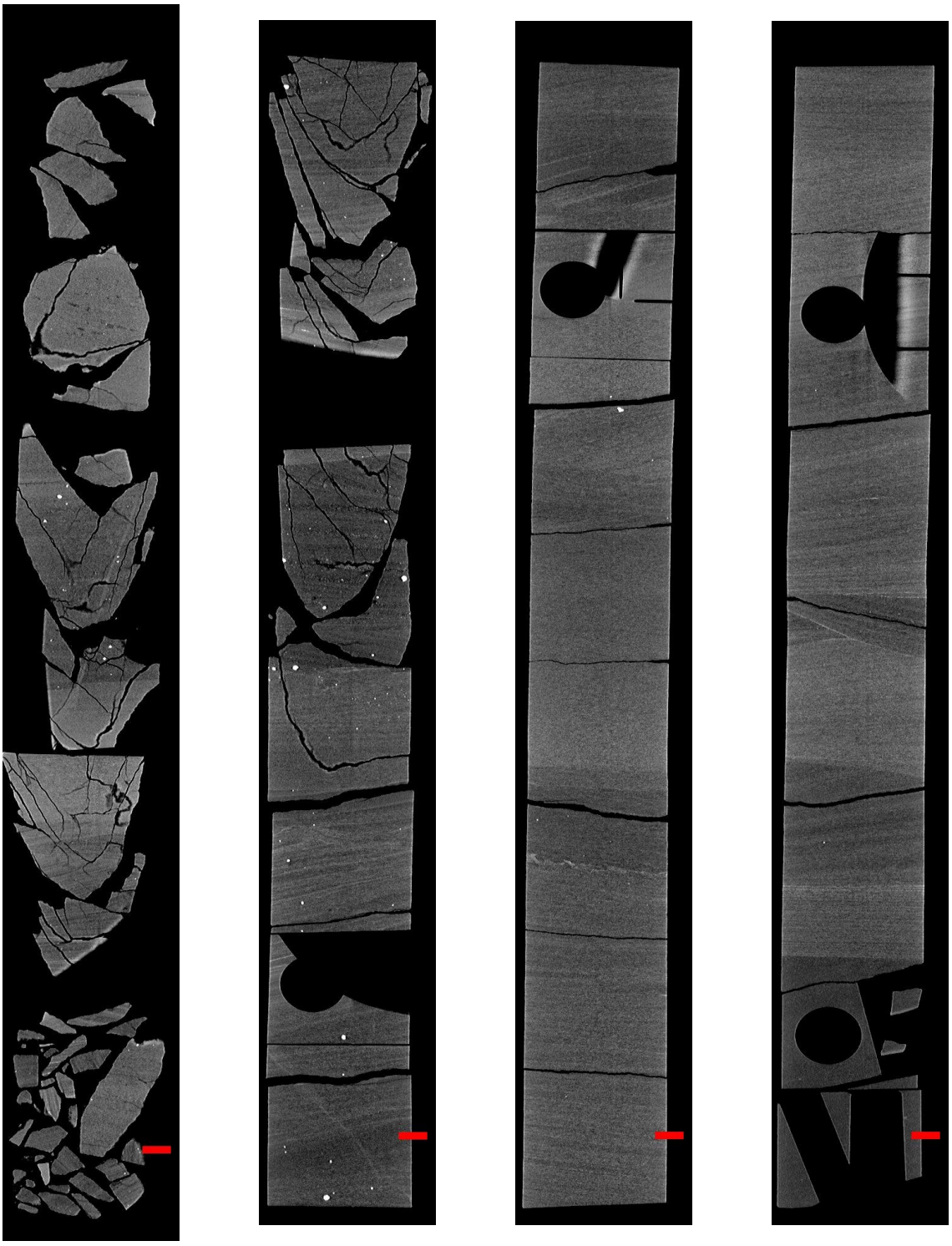

6,400–6,403 ft **6,403–6,406 ft** **6,406–6,409 ft** **6,409–6,412 ft**

Figure 23: 2D midplanes of the medical CT scans of the OEE Well #1 from 6,400–6,412 ft.

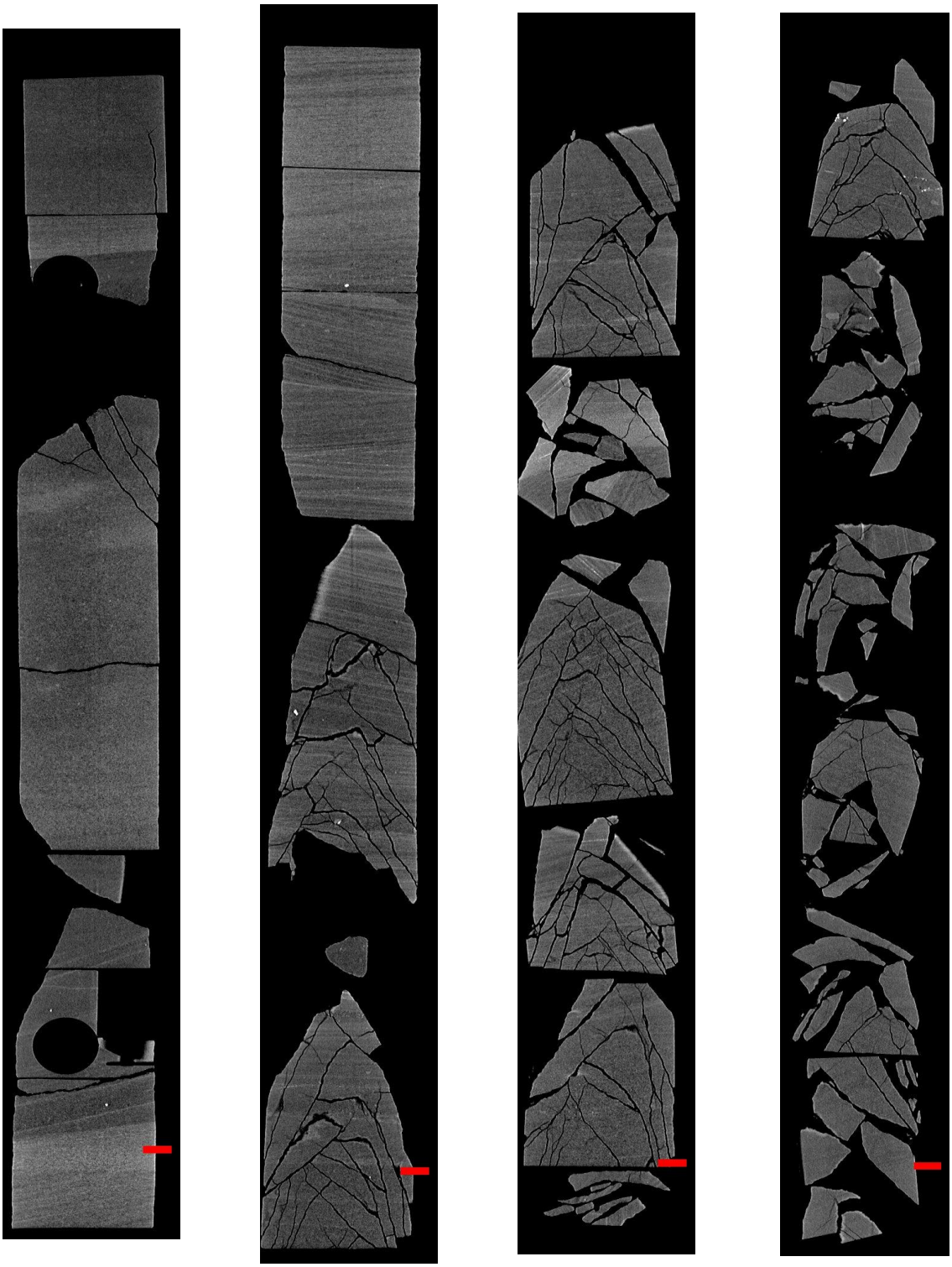

6,412–6,415 ft **6,415–6,418 ft** **6,418–6,421 ft** **6,421–6,424 ft**

Figure 24: 2D midplanes of the medical CT scans of the OEE Well #1 from 6,412–6,424 ft.

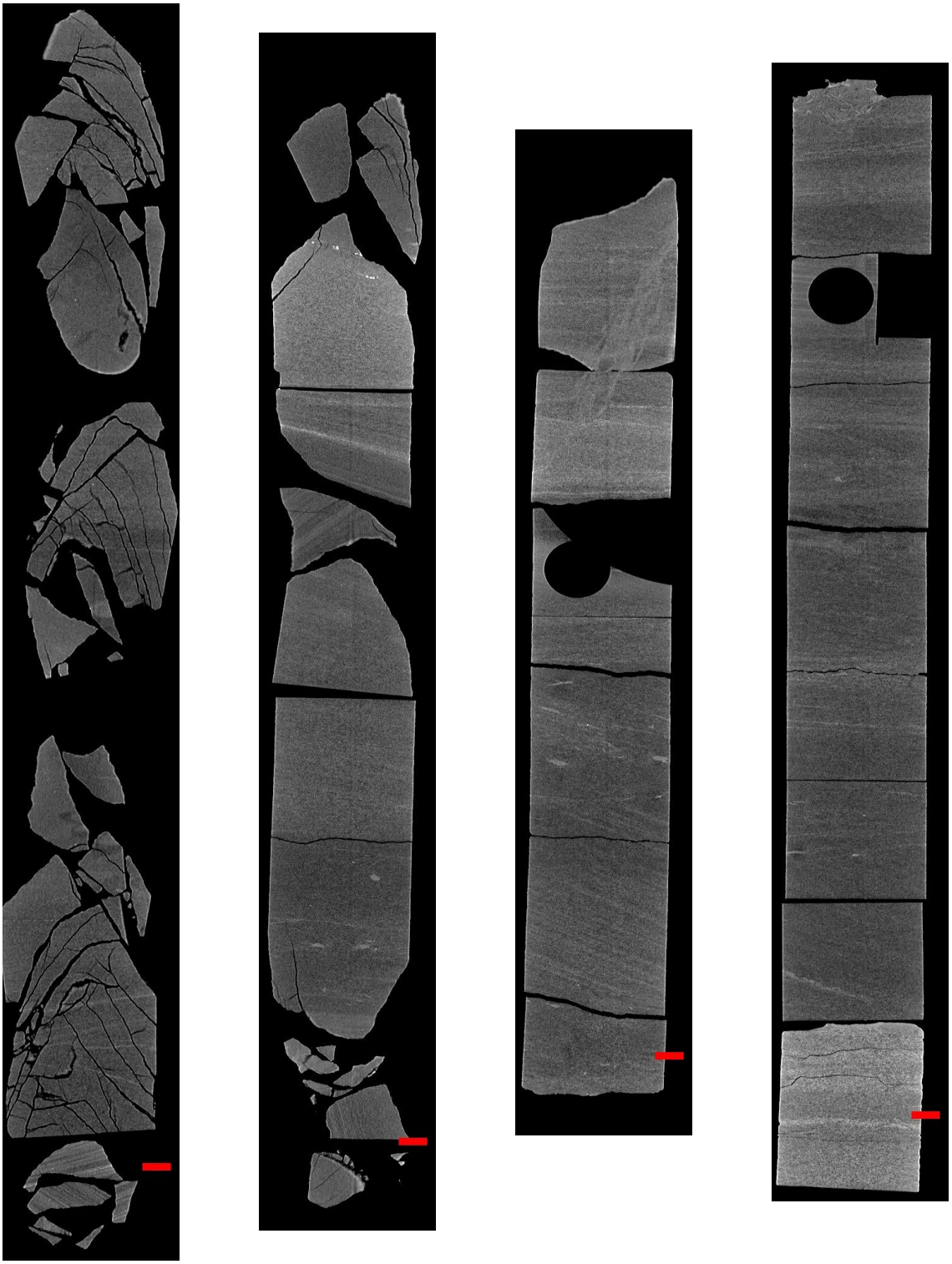

6,424–6,427 ft **6,427–6,430 ft** **6,431–6,434 ft** **6,434–6,436 ft**

Figure 25: 2D midplanes of the medical CT scans of the OEE Well #1 from 6,424–6,436 ft.

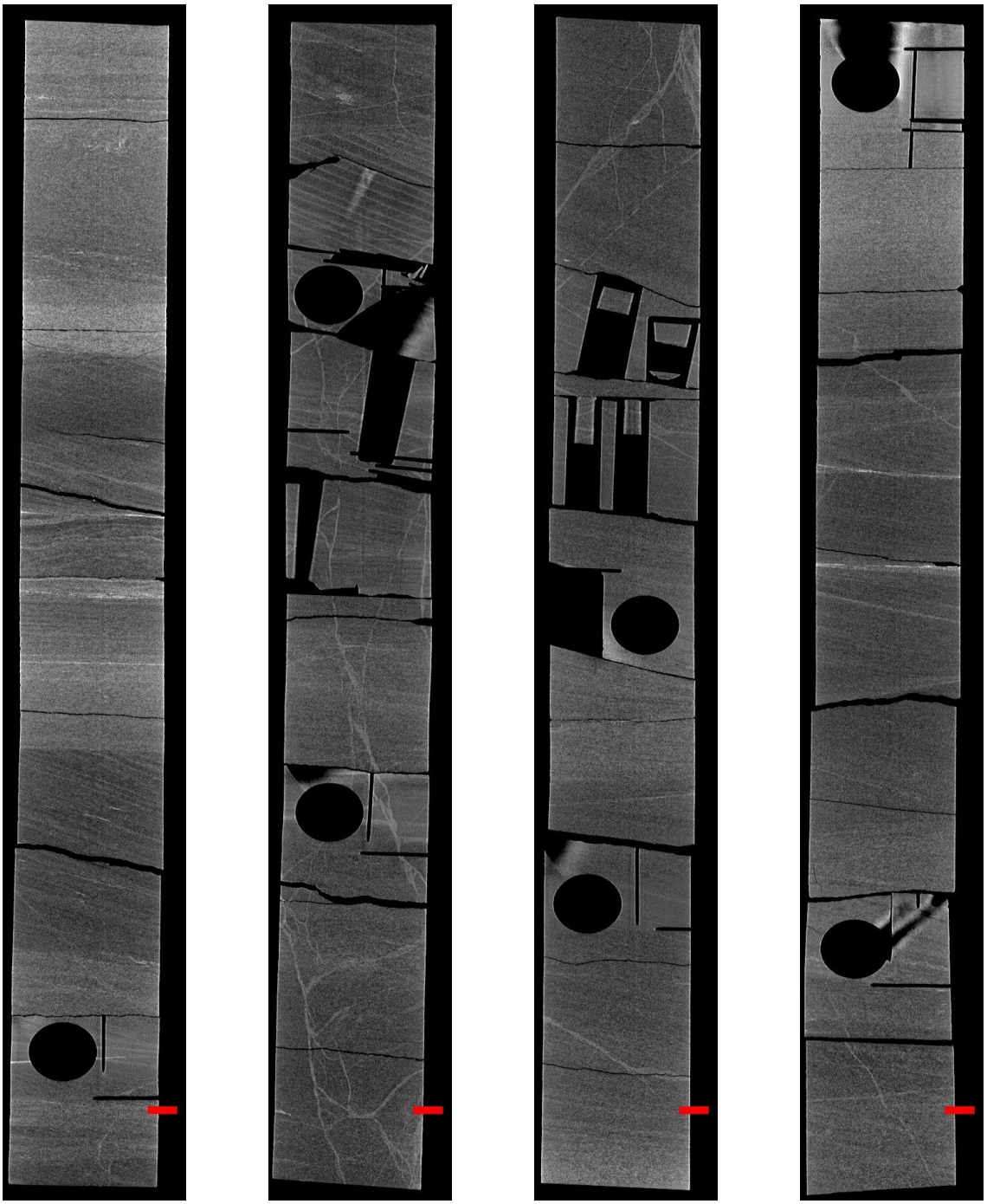

6,436–6,439 ft **6,439–6,442 ft** **6,442–6,445 ft** **6,445–6,448 ft**

Figure 26: 2D midplanes of the medical CT scans of the OEE Well #1 from 6,436–6,448 ft.

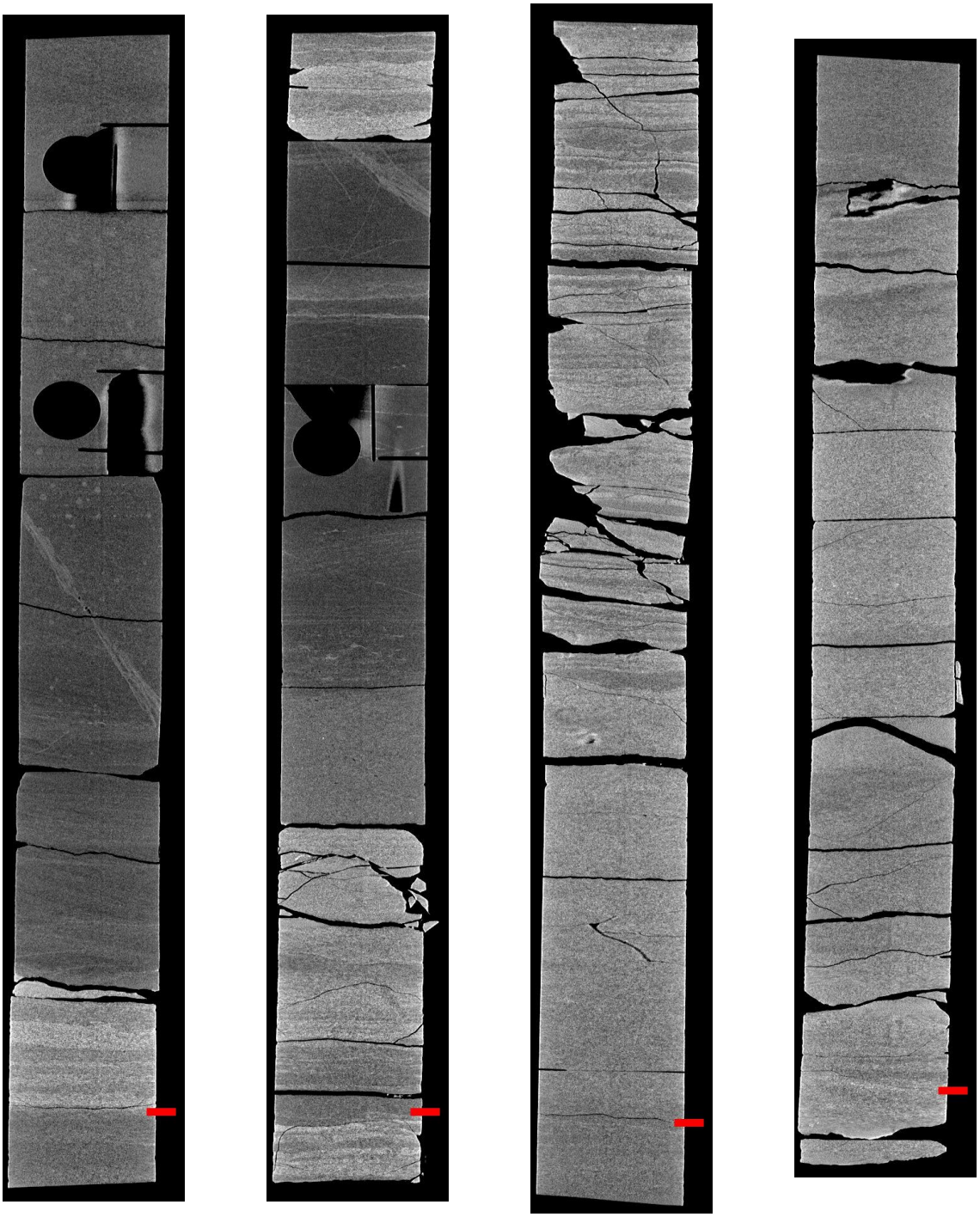

6,448–6,451 ft **6,451–6,454 ft** **6,454–6,457 ft** **6,457–6,460 ft**

Figure 27: 2D midplanes of the medical CT scans of the OEE Well #1 from 6,448–6,460 ft.

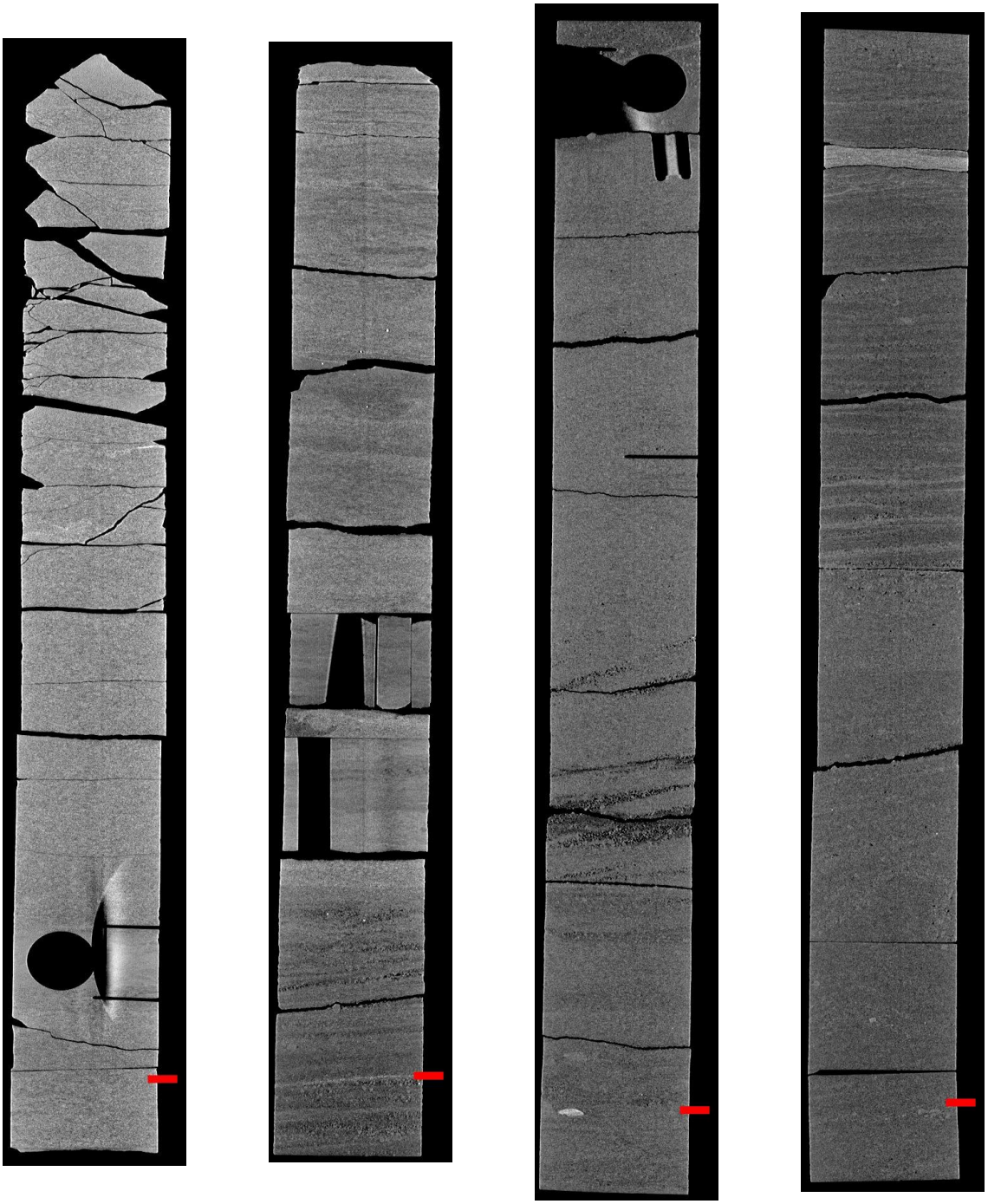

6,460–6,463 ft **6,463–6,466 ft** **6,466–6,469 ft** **6,469–6,472 ft**

Figure 28: 2D midplanes of the medical CT scans of the OEE Well #1 from 6,460–6,472 ft.

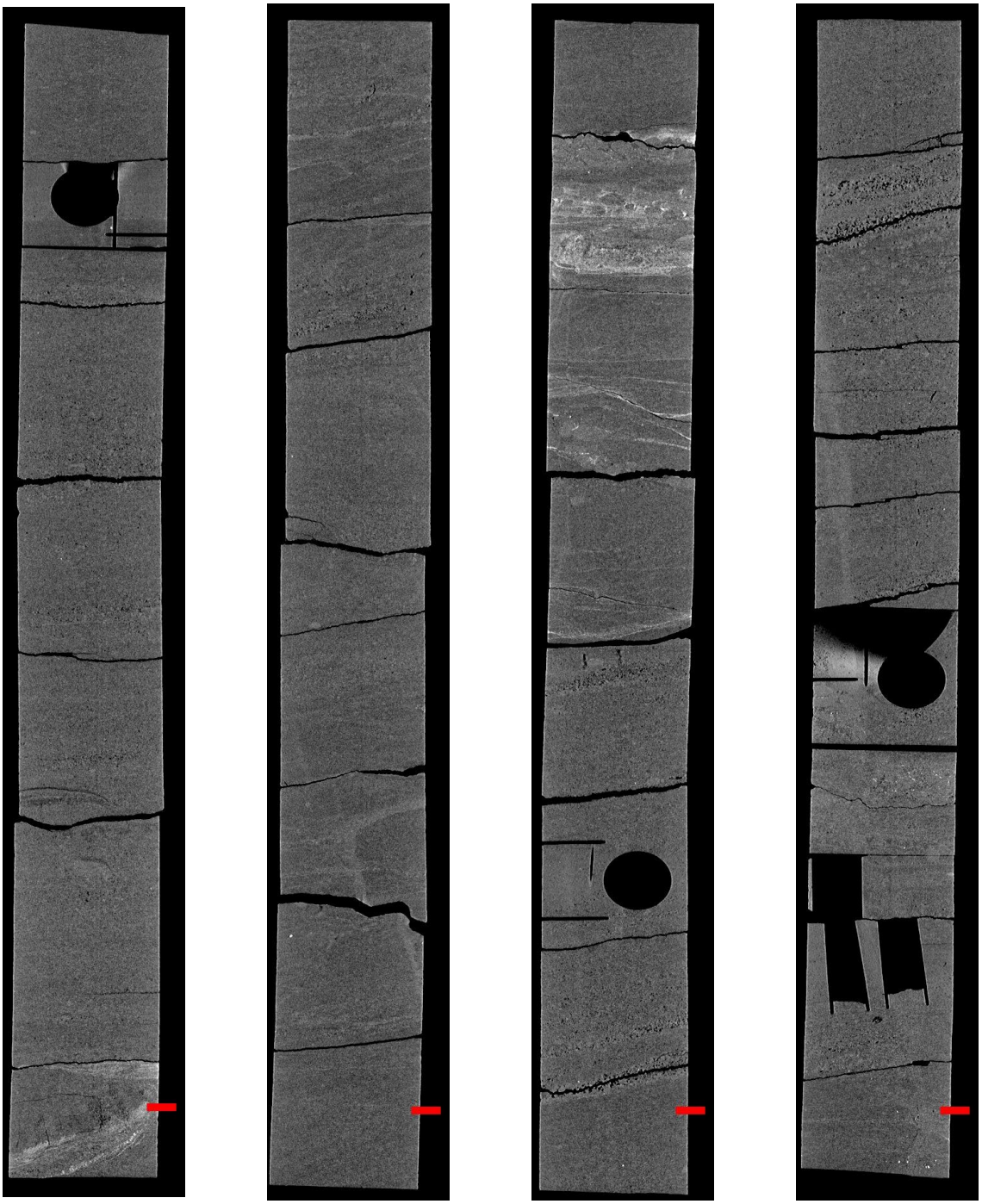

6,472–6,475 ft **6,475–6,478 ft** **6,478–6,481 ft** **6,481–6,484 ft**

Figure 29: 2D midplanes of the medical CT scans of the OEE Well #1 from 6,472–6,484 ft.

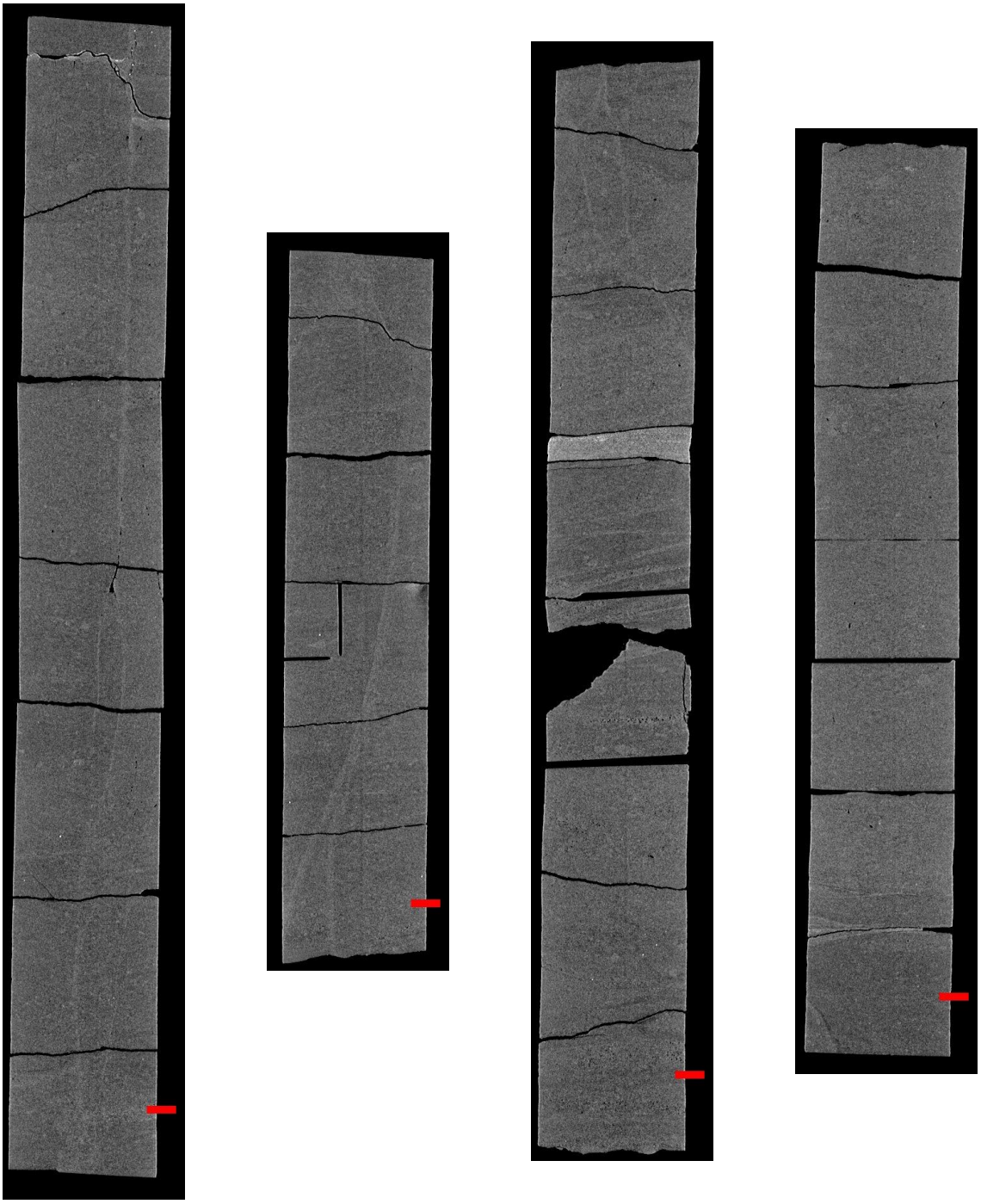

6,484–6,487 ft **6,487–6,489 ft** **6,489–6,491 ft** **6,491–6,494 ft**

Figure 30: 2D midplanes of the medical CT scans of the OEE Well #1 from 6,484–6,494 ft.

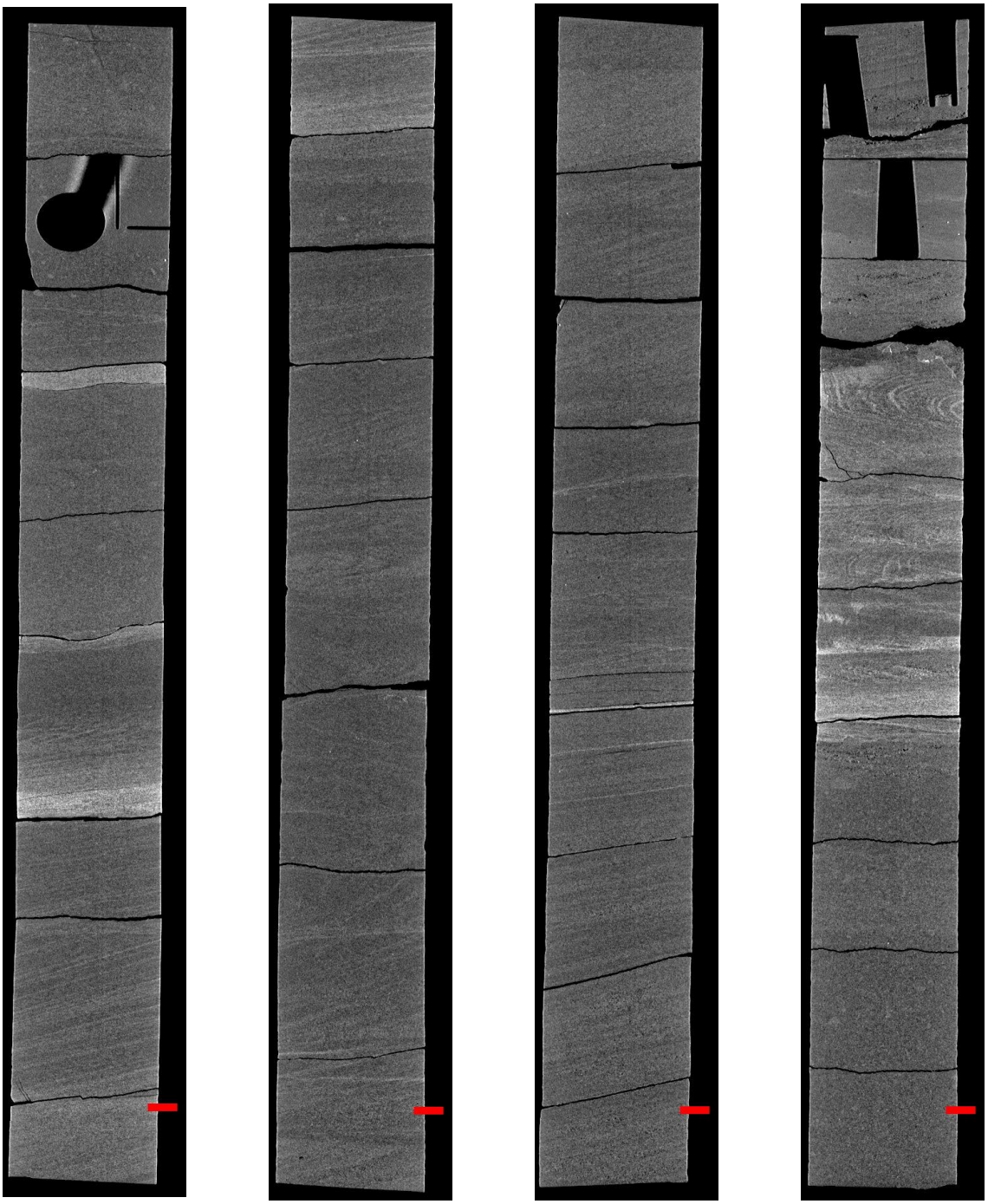

6,494–6,497 ft **6,497–6,500 ft** **6,500–6,503 ft** **6,503–6,506 ft**

Figure 31: 2D midplanes of the medical CT scans of the OEE Well #1 from 6,494–6,506 ft.

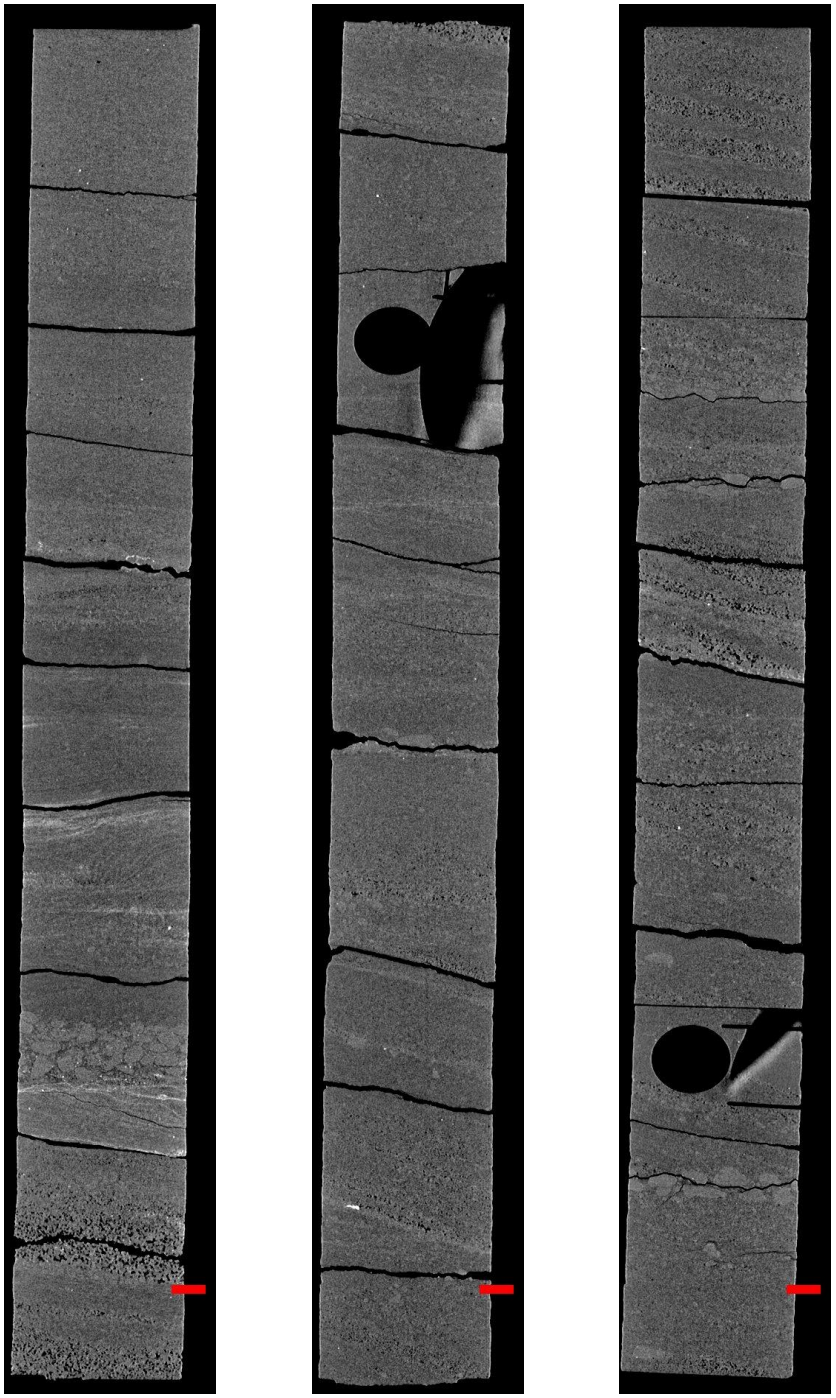

6,506–6,509 ft **6,509–6,512 ft** **6,512–6,515 ft**

Figure 32: 2D midplanes of the medical CT scans of the OEE Well #1 from 6,506–6,515 ft.

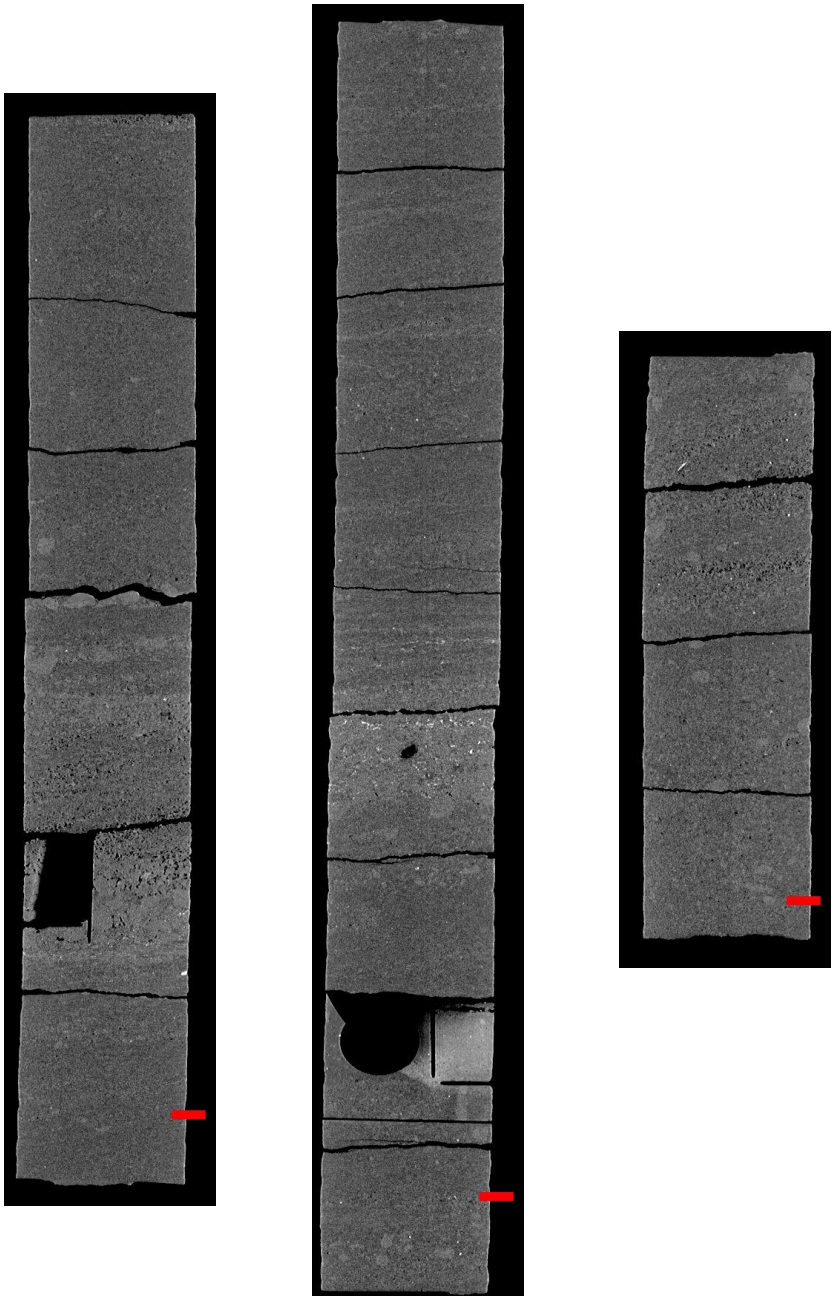

6,515–6,517 ft **6,517–6,520 ft** **6,520–6,521 ft**

Figure 33: 2D midplanes of the medical CT scans of the OEE Well #1 from 6,515–6,521 ft.

4.2 ADDITIONAL CT DATA

Additional CT data can be accessed from NETL's EDX online system using the following link: https://edx.netl.doe.gov/dataset/illinois-storage-corridor-one-earth-energy-1-core. The original CT data is available as 16-bit tif stacks suitable for use with ImageJ (Rasband, 2018) or other image analysis software. In addition, videos showing the variation along the length of the cross-section images shown in the previous section are available for download and viewing. A still image from these videos is shown in Figure 34. The red line through the on the XZ-plane image of the core shows the location of the XY-plane displayed above. The videos on EDX show this XY variation along the entire length of the core.

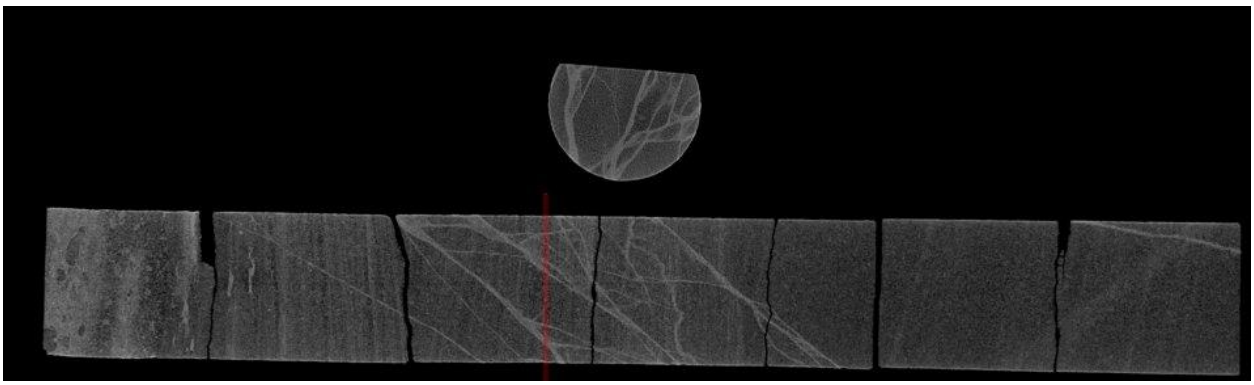

Figure 34: Still from a video file available on EDX showing the medical CT image of the OEE Well #1 core from 6,376 to 6,379 ft. Image shows a dense zone of material in the shallow region, transitioning to a highly laminate sandstone with increasing depth. A dense swarm of mineral filled fractures is observable around 6,377 ft.

4.2.1 Industrial CT Scanning

Detailed scans of sections of interest were performed with NETL's North Star Imagining Inc. M-5000® Industrial CT. The selected core sections are listed in Table 2 along with the voxel resolution and the image title on EDX. Four images through the center of the cores are shown in Figure 35 and Figure 36 as an example of the industrial CT images and full datasets are available on EDX.

Table 2: Industrial CT Images from the OEE Well #1

Depth (ft)	Name on EDX	Voxel Resolution (µm³)
6,438.3	One Earth 6438.3	**62.5**
6,504	One Earth Core 4 Box 26 6504	**62.5**
6,504.4	One Earth Core 4 Box 26 6504.4	**62.5**
6,511.58	One Earth Core 4 Box 29 6511.58	**62.5**

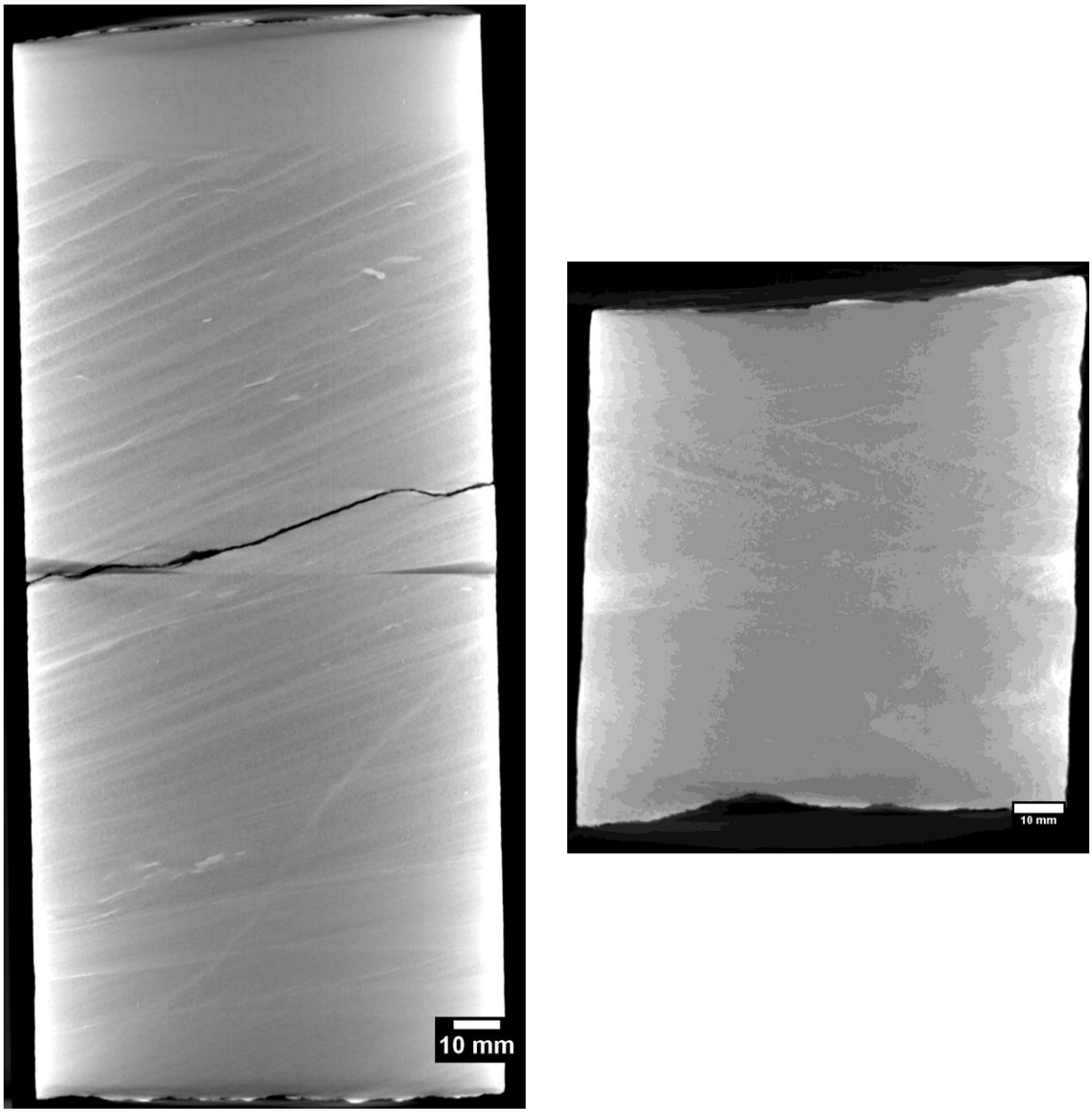

6,438.3 ft **6,504 ft**

Figure 35: OEE Well #1 industrial CT scanner images, samples from 6,438.3 and 6,504 ft.

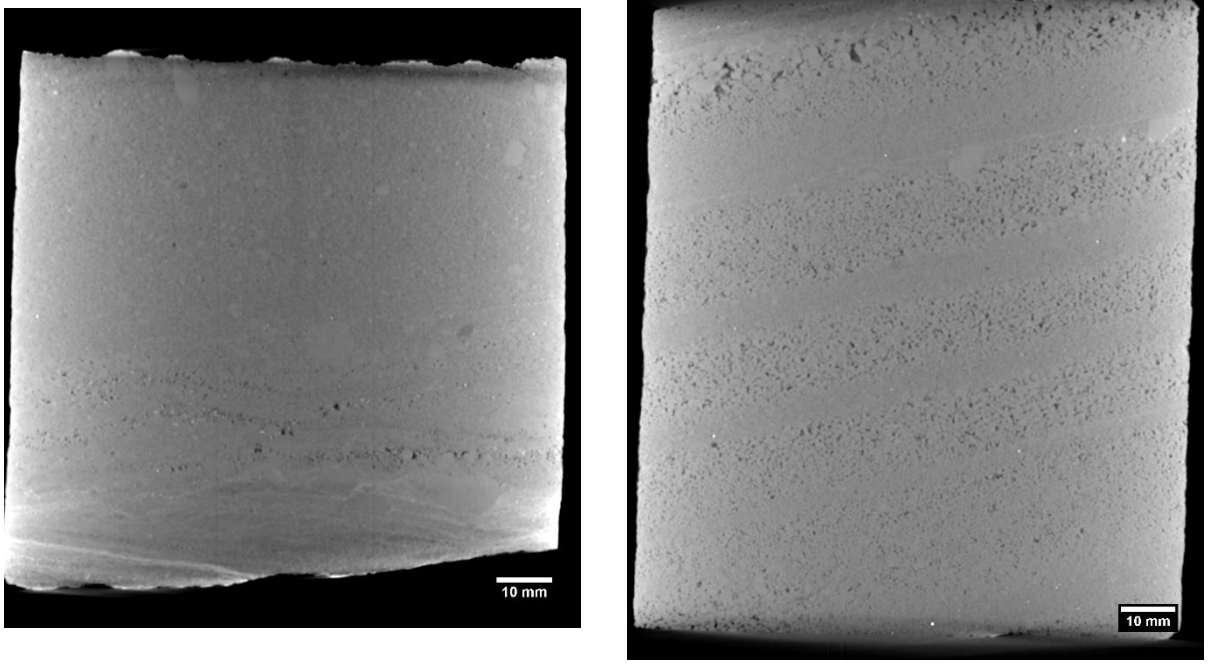

6,504.4 ft **6,511.58 ft**

Figure 36: OEE Well #1 industrial CT scanner images, samples from 6,504.4 and 6,511.58 ft.

4.2.2 Micro CT scanning

Detailed scans of section of interest were preformed using NETL's DynaTOM and Xradia CT scanners. Table 3 and Table 4 list the selected intervals with depth and voxel resolution for each scanner.

Montages of the scans are shown in the images following the tables. Each montage is an illustration of five cross-sections through the core along the length of sample. Full resolution 16-bit tif stacks of these datasets are available on EDX. As these files can be quite large (~15 GB) and difficult to process on standard computers each image stack has been scaled by 50% and converted to an 8-bit tif stack as well, resulting in files that are less than 1 GB and easier to interrogate.

Table 3: Micro CT Images Obtained with the TESCAN DynaTOM

Depth (ft)	Name on EDX	Voxel Resolution (mm^3)
4,366	One Earth C2B21 4366	**34.3**
6,350	One Earth C3B4 6350A	**30.6**
6,350	One Earth C3B4 6350B	**30.6**
6,350.6	One Earth C3B4 6350.6 Bot	**30.6**
6,350.6	One Earth C3B4 6350.6 Top	**30.6**
6,352.7	One Earth C3B4 6352.7	**32.4**

Table 4: Micro CT Images Obtained with NETL's Zeiss Xradia MicroXCT-400 Scanner

Depth (ft)	Name on EDX	Voxel Resolution (μm^3)
6,344	One Earth Core3 Box2 6344	**3.7564**
6,348	One Earth Core3 Box3 6348	**3.7564**
6,351.1	One Earth Core3 Box4 6351.1 - 4x	**3.7564**
6,351.1	One Earth Core3 Box4 6351.1 - M70	**7.9016**
6,356.9	One Earth Core3 Box6 6356.9	**3.7564**
6,371.9	One Earth Core3 Box11 6371.9	**3.7564**
6,400.1	One Earth Core3 Box7 6400.1	**3.7564**
6,420	One Earth Core3 Box27 6420	**3.7564**
6,463.8	One Earth Core4 Box12 6463.8	**3.3722**
6,476.8	One Earth Core4 Box16 6476.8	**3.7564**
6,481.5	One Earth Core4 Box18 6481.5	**3.7564**

The CT scans of the cores using NETL's Tescan DynaTOM micro-CT scanner were obtained with a resolution of approximately 30 microns per voxel, which is an order of magnitude more refined than the medical CT images. At this higher resolution small-scale features not discernable from coarse imaging are more visible, such as the porosity observable in Figure 38 of the core section scanned from OEE Well #1 at a depth of 6,350 ft.

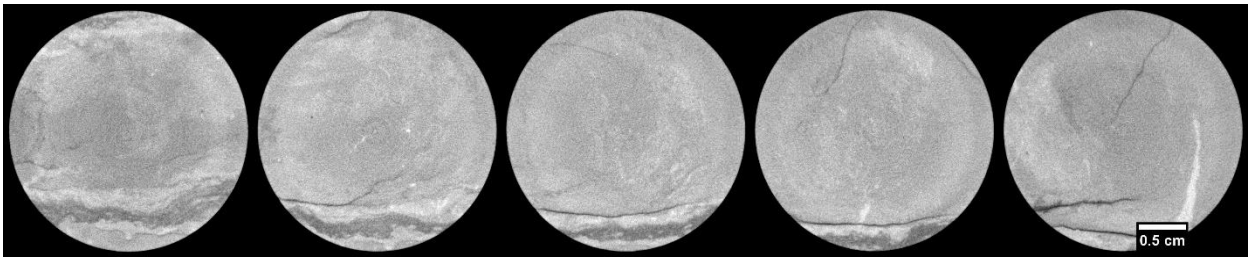

Figure 37: Micro CT image montage from NETL's Tescan DynaTOM micro-CT scanner of the OEE Well #1 from a depth of 4,366 ft.

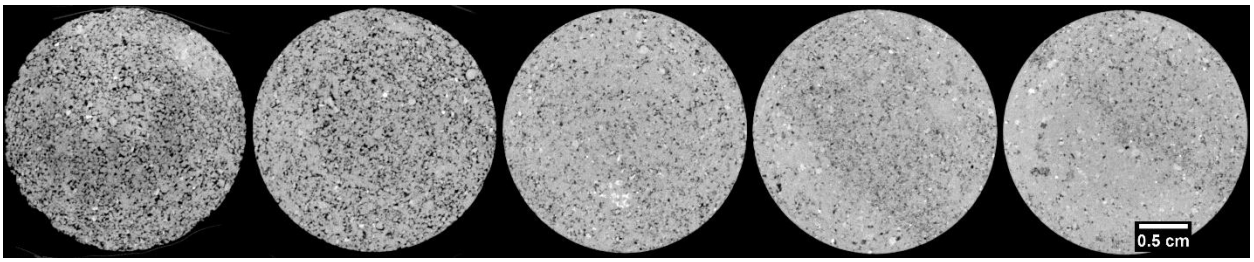

Figure 38: Micro CT image montage from NETL's Tescan DynaTOM micro-CT scanner of the OEE Well #1 from a depth of 6,350 ft.

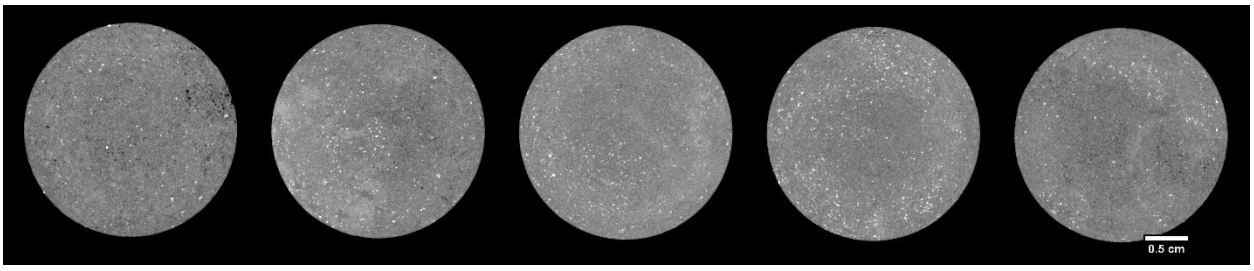

Figure 39: Micro CT image montage from NETL's Tescan DynaTOM micro-CT scanner of the OEE Well #1 from a depth of 6,350.6 ft.

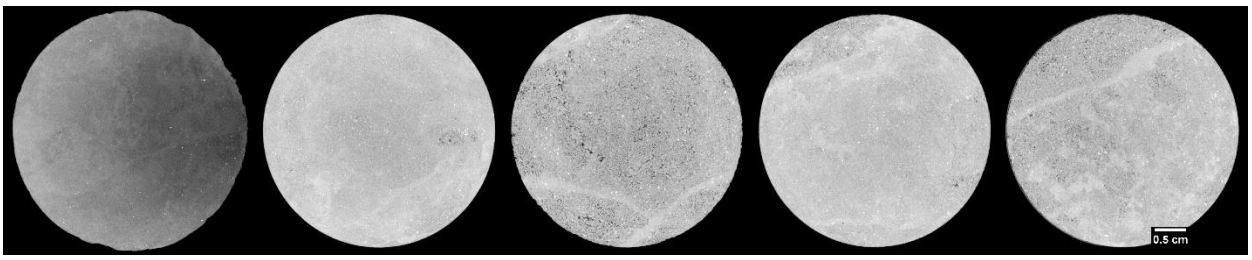

Figure 40: Micro CT image montage from NETL's Tescan DynaTOM micro-CT scanner of the OEE Well #1 from a depth of 6,352.7 ft.

The images obtained with NETL's Zeiss Xradia micro-CT scanner were captured with a resolution of 3 to 7 microns per voxel. At this resolution individual pore spaces and interconnectivity of this porosity is discernable. In addition, micro-fractures in low permeability zones are identifiable at this scale. These features can be seen in the montages in Figure 41 to Figure 51. Full resolution 3D images are available for download and additional analysis from EDX.

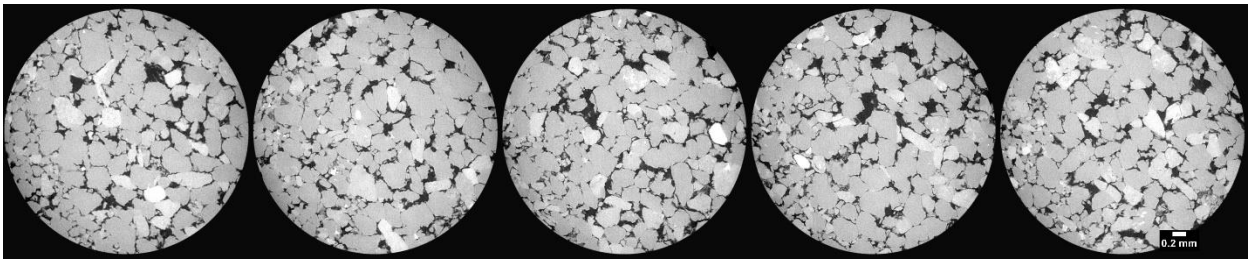

Figure 41: Micro CT image montage from NETL's Zeiss Xradia microXCT-400 scanner of OEE Well #1 from a depth of 6,344 ft.

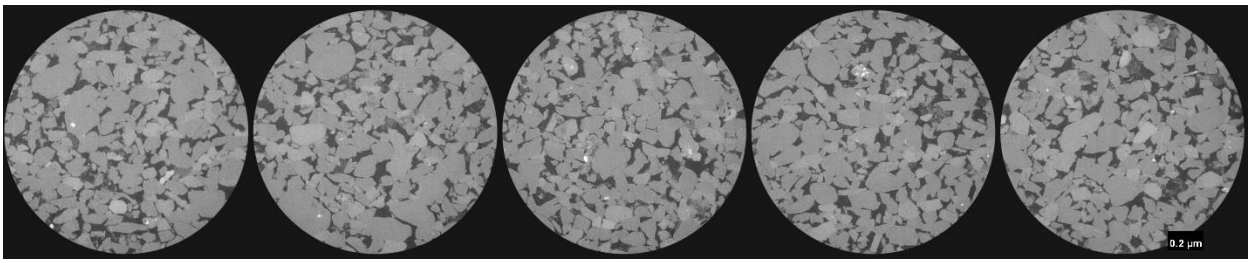

Figure 42: Micro CT image montage from NETL's Zeiss Xradia microXCT-400 scanner of OEE Well #1 from a depth of 6,348 ft.

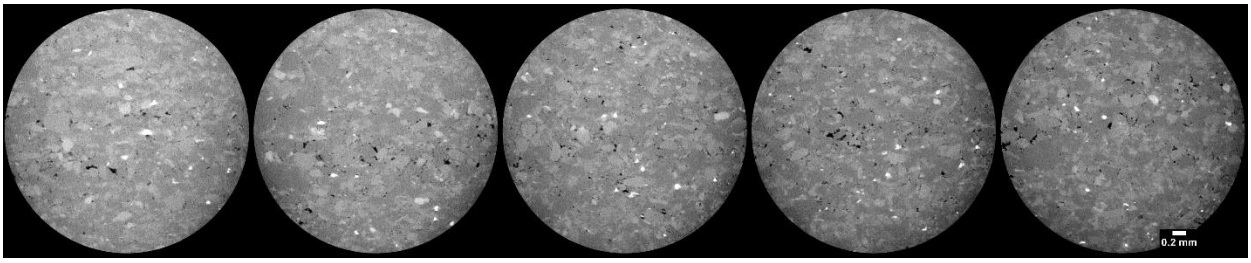

Figure 43: Micro CT image montage from NETL's Zeiss Xradia microXCT-400 scanner of OEE Well #1 from a depth of 6,351.1 ft. Captured with the 4x optics.

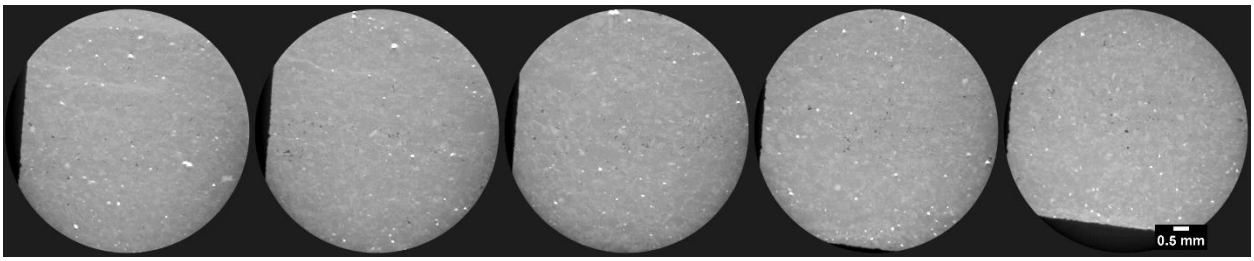

Figure 44: Micro CT image montage from NETL's Zeiss Xradia microXCT-400 scanner of OEE Well #1 from a depth of 6,351.1 ft. Captured with the M70 optics.

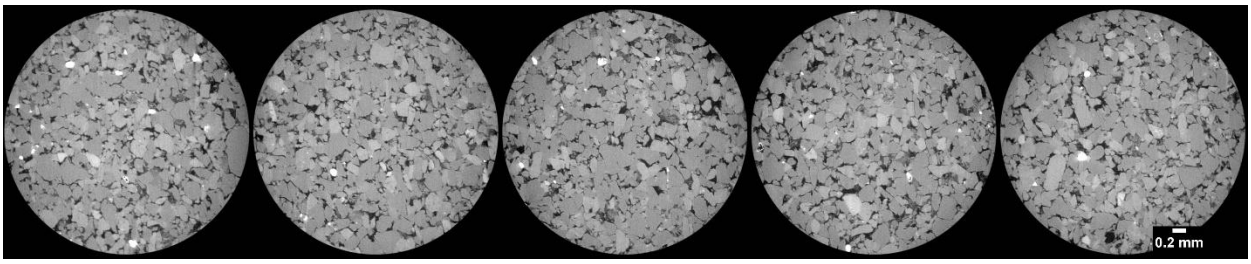

Figure 45: Micro CT image montage from NETL's Zeiss Xradia microXCT-400 scanner of OEE Well #1 from a depth of 6,356.9 ft.

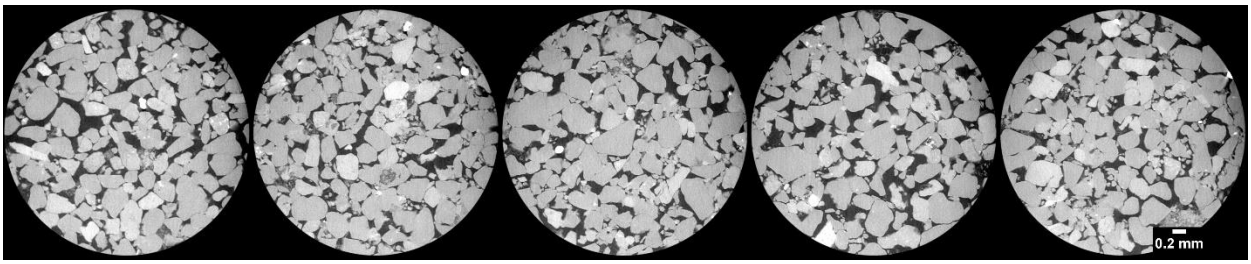

Figure 46: Micro CT image montage from NETL's Zeiss Xradia microXCT-400 scanner of OEE Well #1 from a depth of 6,371.9 ft.

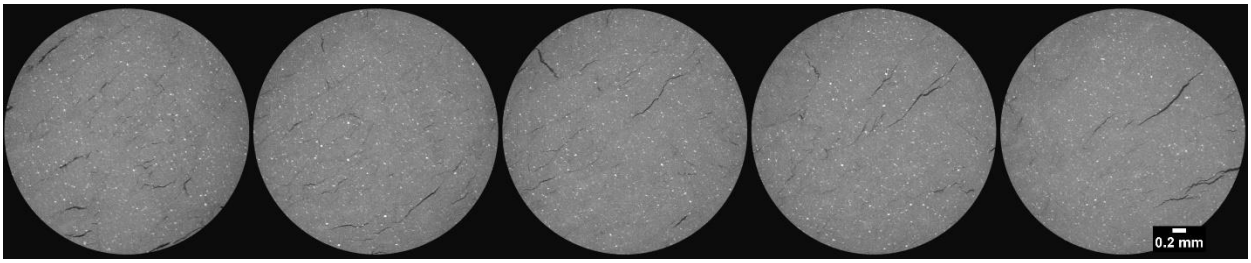

Figure 47: Micro CT image montage from NETL's Zeiss Xradia microXCT-400 scanner of OEE Well #1 from a depth of 6,400.1 ft.

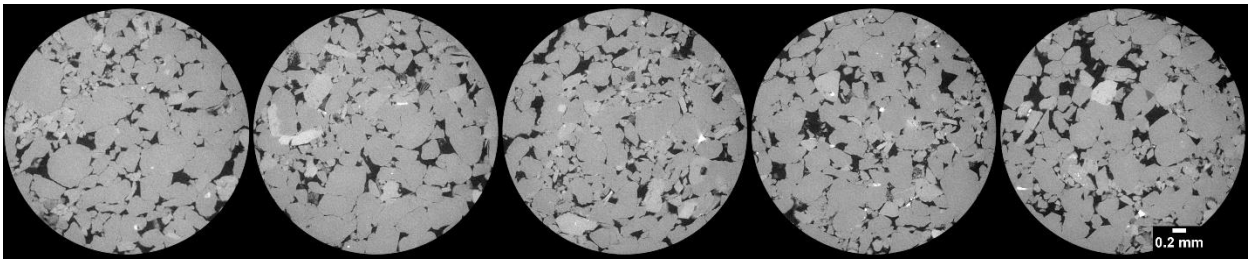

Figure 48: Micro CT image montage from NETL's Zeiss Xradia microXCT-400 scanner of OEE Well #1 from a depth of 6,420 ft.

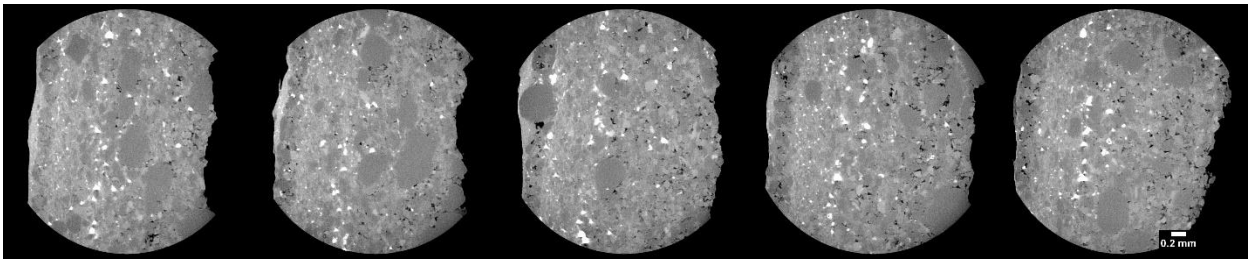

Figure 49: Micro CT image montage from NETL's Zeiss Xradia microXCT-400 scanner of OEE Well #1 from a depth of 6,463.8 ft.

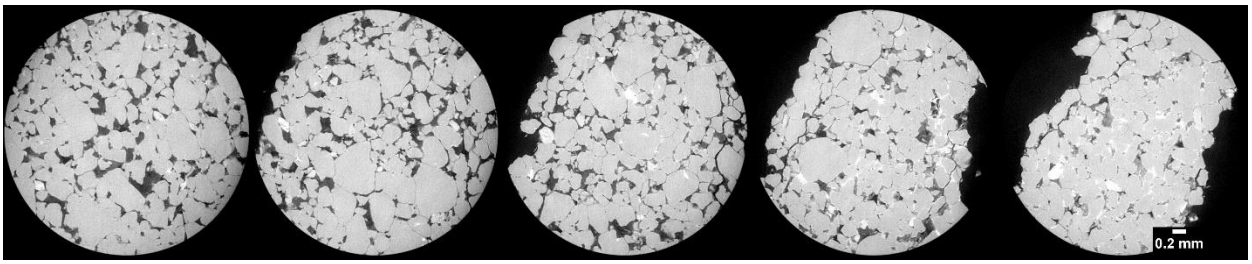

Figure 50: Micro CT image montage from NETL's Zeiss Xradia microXCT-400 scanner of OEE Well #1 from a depth of 6,476.8 ft.

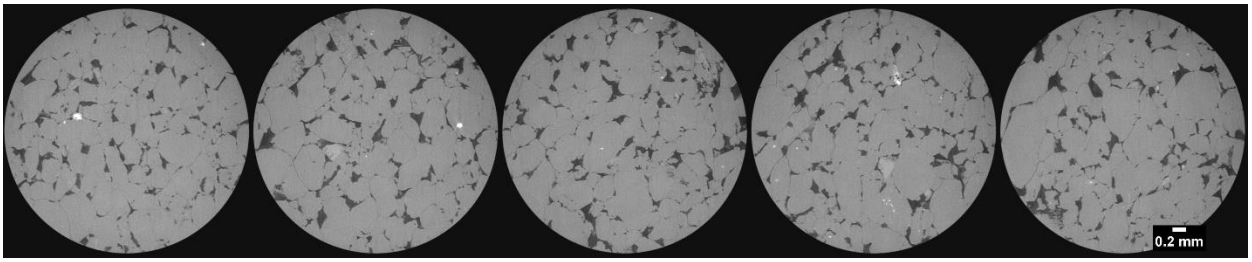

Figure 51: Micro CT image montage from NETL's Zeiss Xradia microXCT-400 scanner of OEE Well #1 from a depth of 6,481.5 ft.

4.3 COMPILED CORE LOG

The compiled core logs were scaled to fit on single pages for rapid review of the combined data from the medical CT and MSCL. The XRF was used to inform geochemical composition and mineralogy. The data is displayed in two plots, the Eau Claire cored section and Mt. Simon cored section (Figure 52 and Figure 53). The Eau Claire shale was sampled at 6 cm spatial resolution for both XRF and petrophysical measurements and used the Olympus Delta XRF (Mining-Plus Suite) for the entirety of the cored interval (Figure 52). The Mt. Simon section included 6 cm resolution sampling from 6,340 to 6,494 ft with petrophysical measurements being measured from 6,340 to 6,494 ft and XRF using the Olympus Delta XRF (Mining-Plus Suite) from 6,340 to 6,370 ft; and 30.48 cm (1 ft) sample resolution from 6,370 to 6,520 ft for XRF elemental distributions using the Olympus Vanta M Series (GeoChem Mode) (Figure 53). The MSCL experienced instrument errors from 6,495 to 6,521 ft in gamma density and magnetic susceptibility measurements, and due to project time constraints, the core was returned to ISGS before those could be addressed and this section remeasured. As such, those tracks are left blank in the combined log shown in Figure 53.

Data from the MSCL was filtered to remove areas of fractures and missing core. The gamma density was limited to values greater than 1.5 g/cm^3.

The elemental results from the XRF are grouped to denote different elemental proxies. These include skeletal influx/carbonate potential (Ca, Mg, and Mn), detrital influence (Zr, Ti, Al, and Si), related to redox potential (Cr, Ni, Cu, Mo, and V), and biogenic production (V).

Additionally, trends in elemental ratios can provide insight into mineral composition, oxidation state, and depositional setting. Examples include: Ca/Si, which provides information on relative abundance of calcium carbonates versus silicates; Mn/Fe, which provides information on oxidation, where a decrease in the ratio is related to zones of anoxic/euxinic conditions and an increase is related to zones of dysoxic/oxic conditions; Ca/Mg, which provides information on dolomite; S/Fe, which provides information on the abundance of pyrite (and other iron sulfates) versus Fe oxide minerals; Fe/Al, which provides information about the degree of pyritization in shales; Ti/Al, which provides information about terrigenous input; and Si/Al, which provides information on the abundance of illite and micas versus other clays. Magnetic susceptibility can test for iron sulfides (reducing) or oxidized Fe and sulfate. The elemental proxy log also includes an XRF “mineralogy” with Al, Fe, and K representing clays; Ca and Mg representing carbonate minerals; and Si, representing only quartz, although there is some Si contribution to the clays. Pyrite (reduced) should have low magnetic susceptibility, and Fe oxide or hydroxide should have high magnetic susceptibility. These broad trends can quickly give information on large suites of core and direct more focused research. These logs are presented in the following images.

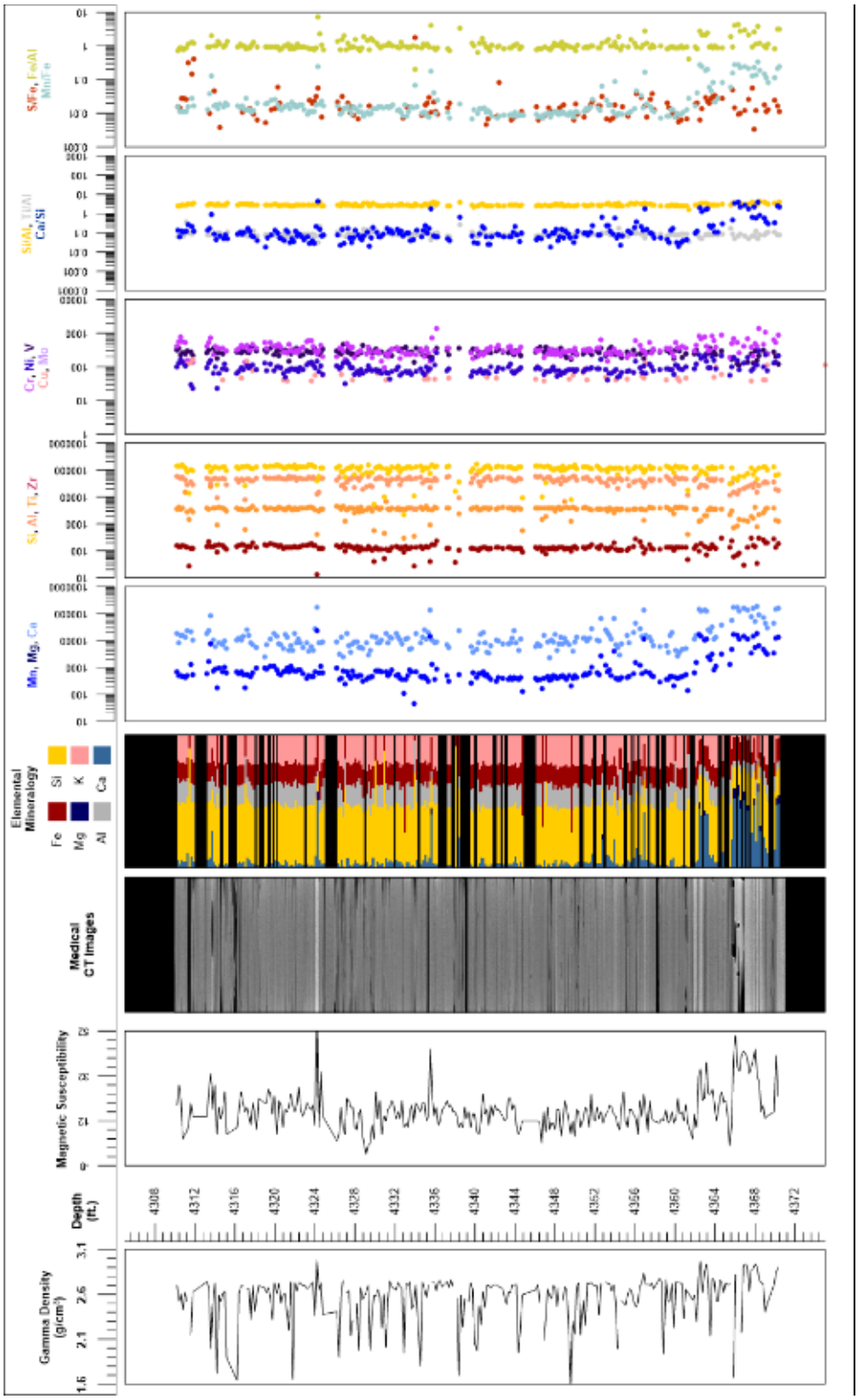

Figure 52: Compiled core log of elemental ratios for the Eau Claire section of the OEE Well #1.

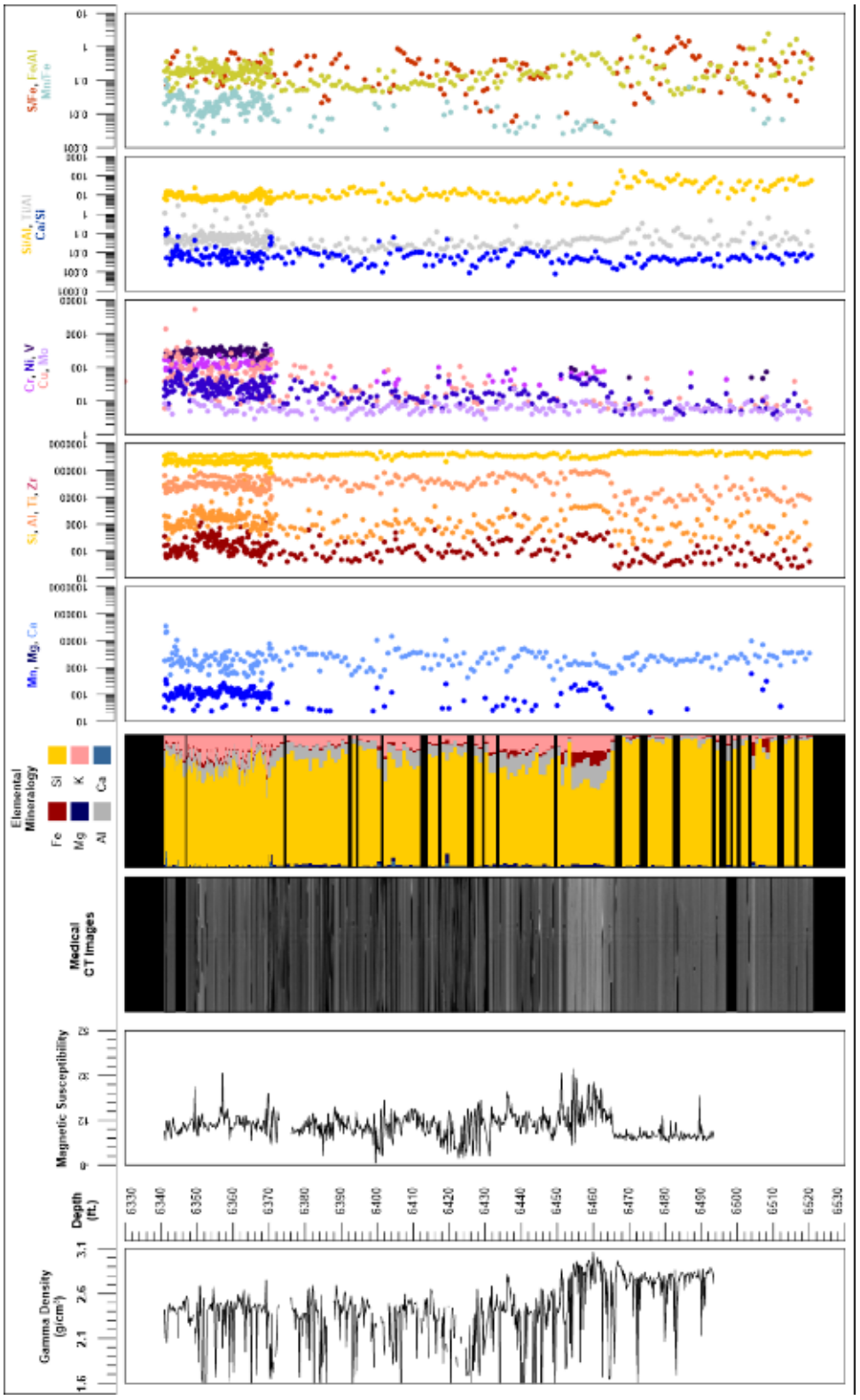

Figure 53: Compiled core log of elemental ratios for the Mt. Simon section of the OEE Well #1.

5. DISCUSSION

The measurements of the magnetic susceptibility, gamma density, P-wave velocity, XRF, and CT analysis provide a unique look into of the internal structure of the core and macroscopic changes in lithology. These techniques:

- Are non-destructive,
- When performed in parallel, give insight into the core beyond what one individual technique can provide,
- Can be used to identify zones of interest for detailed analysis, experimentation, and quantification, and
- Provide a detailed digital record of the core, before any destructive testing or further degradation, that is accessible and can be referenced for future studies.

Datasets for further analysis are available for download from the EDX at https://edx.netl.doe.gov/dataset/illinois-storage-corridor-one-earth-energy-1-core.

6. REFERENCES

Blakley, C.; Carman, C.; Monson, C.; Freiburg, J.; Korose, C. *Developing CO_2 Source and Storage Opportunities across the Illinois Basin Subtask 5.3–Regional Roadmap for Source Network and Storage Deployment Topical Report*; No. DOE/FE002945-8; Univ. of Illinois at Urbana-Champaign, IL, 2019; p.19.

Freiburg, J. T.; Morse, D. G.; Leetaru, H. E.; Hoss, R. P.; Yan, Q. *A depositional and diagenetic characterization of the Mt. Simon Sandstone at the Illinois Basin-Decatur Project carbon capture and storage site, Decatur, Illinois*; 2014.

Freiburg, J. T.; Ritzi, R. W.; Kehoe, K. S. Depositional and diagenetic controls on anomalously high porosity within a deeply buried CO_2 storage reservoir – The Cambrian Mt. Simon Sandstone, Illinois Basin, USA. *International Journal of Greenhouse Gas Control* **2016.** DOI: 10.1016/j.ijggc.2016.11.005.

Freiburg, J.; Delpomdor, F.; McBride, J. H.; Leetaru, H.; Malone, D.; Grigsby, N.; Khosravi, M.; Frailey, S.; Damico, J.; Monson, C.; Askari, Z. *The Geology of The Mt. Simon Sandstone Storage Complex at the Wabash# 1 Well, Vigo Co., Indiana, Subtask 7.2, Technical Report*; No. DOE-FE0031626-9; Univ. of Illinois at Urbana-Champaign, IL, 2022. https://www.osti.gov/servlets/purl/1866412

Geotek Ltd. Multi-Sensor Core Logger Manual; Version 05-10; Published by Geotek, 3 Faraday Close, Daventry, Northamptonshire NN11 8RD, 2010. info@geotek.co.uk, www.geotek.co.uk

Hunts, C.; Moskowitz, B.; Banerjee, S. Magnetic Properties of Rocks and Minerals. *Rock Physics and Phase Relations: A Handbook of Physical Constants*; 1995; p 189–204.

Korose, C.; Whittaker, S. *Wabash CarbonSAFE DE-FE0031626;* Carbon Storage Project Review Meeting; U.S. Department of Energy; National Energy Technology Laboratory; 2020.

Morse, D. G.; Leetaru, H. E. *Reservoir characterization and three-dimensional models of Mt. Simon gas storage fields in the Illinois Basin*; Illinois State Geological Survey: Champaign, IL, 2005.

Nelson, W. J. Structural features in Illinois. *Illinois State Geological Survey Bulletin no. 100;* 1995; p. 153. https://hdl.handle.net/2142/43644

Rasband, W. S. ImageJ. U.S. National Institutes of Health: Bethesda, MD, 1997–2016, http://imagej.nih.gov/ij/ (accessed 2018).

Reesink, A. J. H.; Best, J.; Freiburg, J. T.; Webb, N. D.; Monson, C. C.; Ritzi, R. W. Interpreting pre-vegetation landscape dynamics: The Cambrian Lower Mount Simon Sandstone, Illinois, USA. *Journal of Sedimentary Research* **2020,** *90*, 1614–1641.

Whittaker, S., *Illinois Storage Corridor DE-FE0031892*, 2022 Carbon Management Research Project Review Meeting, PA, 2022. https://netl.doe.gov/sites/default/files/netl-file/22CM_CTS16_Whittaker.pdf (accessed 2023).

Brian J. Anderson
Director
National Energy Technology Laboratory
U.S. Department of Energy

Darin Damiani
Carbon Storage Program Manager
Office of Carbon Management
U.S. Department of Energy

Mark McKoy
Advanced Carbon Technology Manager
National Energy Technology Laboratory
U.S. Department of Energy

Bryan Morreale
Executive Director
Research and Innovation Center
National Energy Technology Laboratory
U.S. Department of Energy

William Aljoe
Carbon Storage Infrastructure Technology Manager
National Energy Technology Laboratory
U.S. Department of Energy

Dawn Deel
Carbon Storage Project Manager
Technology Development Center
National Energy Technology Laboratory
U.S. Department of Energy

NETL Technical Report Series